

Neuronized Priors for Bayesian Sparse Linear Regression

Minsuk Shin

Harvard Data Science Initiative, Harvard University

and

Jun S Liu

Department of Statistics, Harvard University

Abstract

Although Bayesian variable selection procedures have been widely adopted in many scientific research fields, their routine use in practice has not caught up with their non-Bayesian counterparts, such as Lasso, due to difficulties in both Bayesian computations and in testing effects of different prior distributions. To ease these challenges, we propose the neuronized priors to unify and extend existing shrinkage priors such as one-group continuous shrinkage priors, continuous spike-and-slab priors, and discrete spike-and-slab priors with point-mass mixtures. The new priors are formulated as the product of a weight variable and a scale variable. The weight is a Gaussian random variable, but the scale is a Gaussian variable controlled through an activation function. By altering the activation function, practitioners can easily implement a large class of Bayesian variable selection procedures. Compared with classic spike and slab priors, the neuronized priors achieve the same explicit variable selection without employing any latent indicator variable, which results in more efficient MCMC algorithms and more effective posterior modal estimates obtained from a simple coordinate-ascent algorithm. We examine a wide range of simulated and real data examples and also show that using the “neuronization” representation is computationally more or comparably efficient than its standard counterpart in all well-known cases.

Keywords: Bayesian shrinkage; spike-and-slab prior; variable selection; scalable Bayesian computation.

1 Introduction

We consider the Bayesian linear regression problem in high dimensions. Suppose a model, from which we assume that the observed data $\mathbf{y} = \{y_1, \dots, y_n\}^\top$ are generated, contains p unknown coefficients denoted by $\boldsymbol{\theta} = \{\theta_1, \dots, \theta_p\}^\top$. Here the linear model is

$$\mathbf{y} = X\boldsymbol{\theta} + \epsilon, \quad (1)$$

where X is the $n \times p$ covariate matrix and $\boldsymbol{\theta} \in \mathbb{R}^p$, and $\epsilon \sim N(0, \sigma^2 \mathbf{I})$. Under the sparsity assumption on $\boldsymbol{\theta}$, we typically impose a shrinkage prior on each coefficient. A popular choice is the one-group (continuous) shrinkage prior, which we refer to as the “continuous shrinkage prior” here. It can be constructed via a product of independent hierarchical Gaussian mixture distributions:

$$\begin{aligned} \theta_j \mid \tau_w^2 \tau_j^2 &\sim N(0, \tau_w^2 \tau_j^2) \\ \tau_j &\sim \pi_\tau \text{ and } \tau_w \sim \pi_g, \end{aligned} \quad (2)$$

for $j = 1, \dots, p$, where π_τ and π_g are some densities chosen by the user. The variance parameter τ_j^2 that governs the shrinkage level of individual parameter is called the local shrinkage parameter, and the variance parameter τ_w^2 that controls the overall shrinkage effect is called the global shrinkage parameter (Polson & Scott 2010).

There have been numerous choices of π_τ considered to induce shrinkage on the parameters. These priors include the Bayesian Lasso (Park & Casella 2008) with π_τ being an exponential distribution, the horseshoe prior (Carvalho et al. 2010) with π_τ being a half-Cauchy distribution, the generalized double Pareto (Armagan et al. 2013) with π_τ being a mixture of Laplace distributions, and the Dirichlet-Laplace prior (Bhattacharya et al. 2015) with π_τ being the distribution for the product of a Dirichlet and a Laplace random variables. Recently, theoretical properties of the prior choice for τ_j have been investigated, and the results show that the marginal prior density of θ_j with a heavy tail and a sufficient mass around zero achieves the minimax optimal rate of posterior contraction (Ghosh et al. 2017, van der Pas et al. 2016), like point-mass mixtures of spike and slab priors that will be introduced later.

In Gaussian linear regression models, MCMC sampling of θ_j given the local and global shrinkage parameters can be efficiently implemented by taking advantage of the conjugacy. However, while the continuous shrinkage priors have computational advantages over point-mass priors, their posterior approximation is still difficult in high-dimensional settings. Also, the resulting posterior samples do not automatically provide sparse estimates of the coefficients, so that extra steps are required for variable selection (Hahn & Carvalho 2015).

Another popular class of shrinkage priors is the class of two-group mixture priors, called the *spike-and-slab* (SpSL) priors (Mitchell & Beauchamp 1988, George & McCulloch 1993). These prior densities are represented by a mixture of two densities as follows:

$$\begin{aligned}\theta_j \mid \gamma_j &\sim (1 - \gamma_j)\pi_0(\theta_j) + \gamma_j\pi_1(\theta_j) \\ \gamma_j &\sim \text{Bernoulli}(\eta),\end{aligned}\tag{3}$$

for a hyperparameter η and $j = 1, \dots, p$. The density function π_0 is typically chosen to be highly concentrated around zero so that the shape is spiked at zero, whereas π_1 is relatively disperse (the slab part). When $\gamma_j = 0$, the parameter θ_j is strongly forced to shrink towards zero, and when $\gamma_j = 1$, the prior imposed on θ_j should have a minimal shrinkage effect. Throughout this article, when a point mass density on zero is used for π_0 , we refer to the resulting prior as the “discrete SpSL prior”, and we refer to the SpSL prior with a non-degenerate π_0 as the “continuous SpSL prior”.

Common choices for π_0 and π_1 are Gaussian distributions with a small and a large variance, respectively (George & McCulloch 1993, 1997, Narisetty & He 2014). The role of η is to control the sparsity, and it supervises how many parameters are significant (Scott & Berger 2010). Under some regularity conditions, it has been shown that an appropriate choice of η leads to model selection consistency (Narisetty & He 2014) and the optimal posterior contraction (Castillo et al. 2012, 2015) for high-dimensional linear regression and normal mean models. However, its computational implementation is challenging due to the adoption of the binary latent variable. In particular, when a point-mass prior on zero is used as π_0 , the approximation of the posterior distribution of the γ_j ’s is notoriously challenging. MCMC sampling strategies (Dellaportas et al. 2002, Guan & Stephens 2011) and stochastic search strategies (Hans et al. 2007, Berger & Molina 2005, Zhang et al. 2007) have been proposed to attack the computational difficulty, mostly relying on the conjugacy of each component of the prior. However, a computational strategy for general discrete SpSL priors such as those using reversible jump proposals (Green 1995) is rarely practical especially under high-dimensional settings.

As a computationally scalable implementation of continuous SpSL priors, Rockova & George (2014) proposed the Expectation Maximization Variable Selection (EMVS), which is an EM algorithm to evaluate the *maximum a posteriori* (MAP) estimator of the regression coefficients under continuous SpSL priors with Gaussian components, and Rockova & George (2018) extended their idea to the spike-and-slab Lasso (SSLasso) prior by adopting Laplace distributions for π_0 and π_1 . These procedures, however, provide only point estimates, and are insufficient in quantifying the uncertainty in model selection and estimation.

To address these computational and practical issues from the shrinkage priors, we propose *neuronized priors*, which provides a unified form of shrinkage priors including as special cases continuous shrinkage priors, continuous SpSL priors, and discrete SpSL priors. In the form of neuronized priors, each parameter is reparameterized as a product of a weight parameter and a transformed scale parameter via an activation function. We define the proposed prior as follows:

Definition 1.1. (Neuronized prior) *For a nondecreasing activation function T and a pre-fixed hyperparameter α_0 , a neuronized prior for θ_j is defined as:*

$$\theta_j := T(\alpha_j - \alpha_0)w_j, \quad (4)$$

where the scale parameter α_j follows $N(0, 1)$ and the weight parameter w_j follows $N(0, \tau_w^2)$ for a hyperparameter τ_w , and $j = 1, \dots, p$.

As the name implies, this formulation is inspired by the use of activation function in neural network models (Rosenblatt 1958, Rumelhart et al. 1986). However, unlike neural network models, the proposed formulation is fully parametric, and it retains clear interpretability on the regression coefficients. In neuronized priors, we use an activation function T in the formulation of shrinkage priors, and show that, for most existing shrinkage priors, we can find specific activation functions such that the resulting neuronized priors correspond to the existing ones. As a consequence, existing theoretical properties of various shrinkage priors can be exactly applied to posterior behaviors based on the neuronized priors. This theoretical equivalence will be discussed in Section 2. We also show that variable selection procedures based on neuronized priors attain the following advantages over existing shrinkage priors:

- *Unification.* Without changing computational algorithms, various classes of shrinkage priors can be practically implemented by just changing the activation function. This characteristic significantly reduces practical and computational efforts to migrate from one shrinkage prior to another in a different class, e.g., from a horseshoe prior to a discrete SpSL prior. It is of practical value and importance to scientists who adopt a Bayesian variable selection procedure to examine effects of different prior choices and our Bayesian computational procedure with neuronized priors can certainly help with this effort. In Table 1 in Section 2, we provide details regarding how a choice of the activation function connects the corresponding neuronoized prior to a commonly considered shrinkage prior.

- *Efficient MCMC implementation.* By formulating the discrete SpSL prior as a neuronized prior using a Rectifier Linear Unit (ReLU) activation function ($T(t) = \max\{0, t\}$; Glorot et al. 2011), we can significantly improve the computational efficiency of the corresponding Bayesian variable selection procedure under high-dimensional settings (Section 2). Moreover, neuronized versions of continuous shrinkage priors also attain comparable or better efficiency in the corresponding MCMC sampling compared with the standard procedures.
- *Scalable optimization to evaluate the MAP estimator.* For massive data sets, MCMC algorithms are often less practical, and one needs to consider the problem of finding the MAP estimator. To achieve this end, we propose an efficient coordinate-ascent optimization algorithm. Unlike EMVS of Rockova & George (2014), the proposed procedure can be applied to a more general class of shrinkage priors including continuous shrinkage priors, continuous and discrete SpSL priors. Compared with the Majorization-Minimization (MM) method of Yen et al. (2011), the EMVS, and the SSLasso, the proposed algorithm with a warm start performed much better in finding the MAP estimator for the notoriously challenging regression problem with discrete SpSL priors (Section 4.3).

We will demonstrate the neuronized counterparts of three popular shrinkage priors for Bayesian sparse regression in Section 2: the discrete SpSL, the Bayesian Lasso, and the horseshoe prior. In Section 3, we show how to manage the neuronized prior so as to achieve one’s intended goals, such as matching a given prior or controlling the prior sparsity. We describe two main advantages of using neuronized priors in Section 4: more efficient MCMC sampling and more effective mode-finding. In Section 5, we cover a wide range of simulation studies to compare the effects of different priors and provide evidences showing that Bayesian solutions with discrete SpSL priors and their neuronized counterparts tend to perform better than other approaches when signal is weak to modest. Two real data examples are analyzed in Section 6, and a short conclusion is given in Section 7. All proofs of main results are provided in Appendix.

2 Connections of Neuronized Priors to Existing Priors

2.1 Discrete SpSL prior

Consider the ReLU (or hinge) activation function. When $\alpha_0 = 0$ and $p = 1$, since $\alpha \sim N(0, 1)$, it is clear that the distribution of $T(\alpha)$ follows an equal mixture of the point-mass

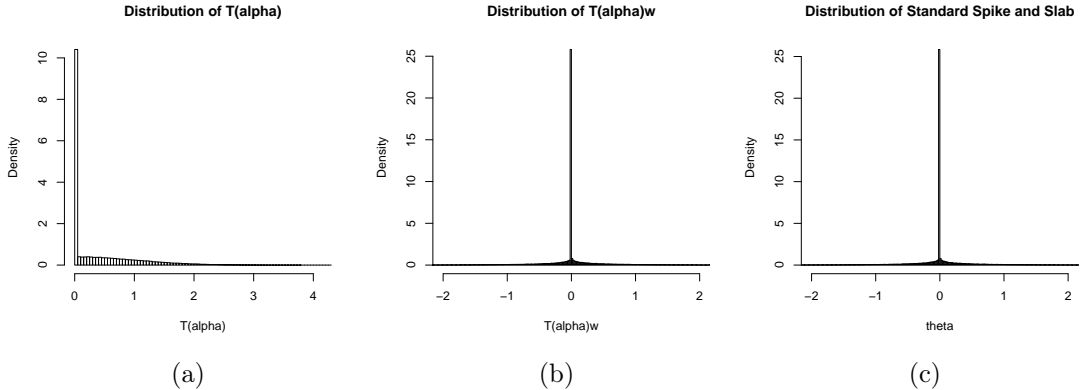


Figure 1: (a) histogram of $T(\alpha)$; (b) histogram of $T(\alpha)w$; (c) histogram of the standard SpSL prior in (5).

at zero and the half standard Gaussian, as shown in Figure 1(a). This implies that the marginal density of $T(\alpha)w$ on Figure 1(b) is equivalent to the standard discrete SpSL prior (Figure 1(c)), and can be written as

$$\begin{aligned} \theta | \gamma &\sim (1 - \gamma)\delta_0(\theta) + \gamma\pi(\theta) \\ \gamma &\sim \text{Bernoulli}(1/2), \end{aligned} \tag{5}$$

where π is the marginal density of the product of two independent standard Gaussian random variables, which can be shown to have an exponential tail.

In general, the hyperparameter α_0 controls the prior probability of sparsity. Since $\alpha \sim N(0, 1)$, it follows that $P(T(\alpha - \alpha_0) = 0) = P(\alpha < \alpha_0) = \Phi(\alpha_0)$, where Φ is the standard Gaussian CDF. More precisely, setting $\gamma \sim \text{Bernoulli}(\Phi(-\alpha_0))$ in (5) results in the same prior as the neuronized prior corresponding to α_0 . Conversely, given $0 < \eta < 1$, we choose $\alpha_0 = -\Phi^{-1}(\eta)$ to result in the desired neuronized prior.

When $p > 1$, theoretical results for discrete SpSL priors are well-studied, and Castillo et al. (2012) and Castillo et al. (2015) considered a class of hyperpriors on the proportion parameter in the Bernoulli variable in (3). That is

$$\eta \sim \text{Beta}(1, p^a), \tag{6}$$

where $a > 1$. By using this prior on η , they investigated model selection consistency and posterior contraction rate related to the choice of η (α_0 for the neuronized prior) under linear

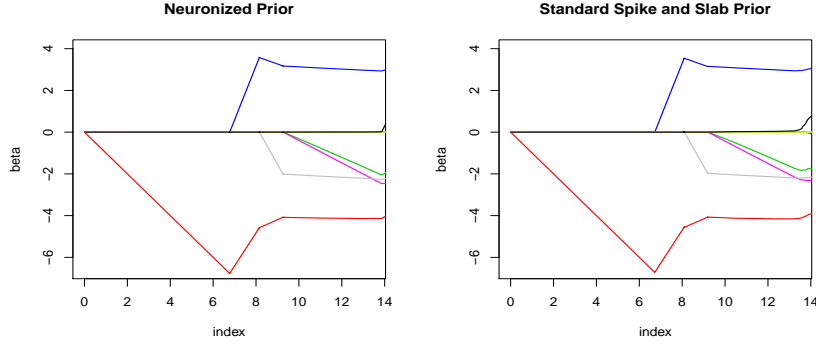


Figure 2: Solution paths of the neuronized prior and the discrete SpSL prior.

regression models. The same theoretical claims can be applied to the neuronized prior with a ReLU activation function by choosing $\alpha_0 = -\Phi^{-1}((p + p^a)^{-1})$. This connection is due to the fact $\pi(\gamma) \propto \int_0^1 \eta^s (1 - \eta)^{p + p^a - s - 1} d\eta = (p + p^a - s)^{-1} \binom{p + p^a}{s}^{-1}$, where $s = \sum_{j=1}^p \gamma_j$, so it follows that $\pi(\gamma_j = 1) \asymp (p + p^a)^{-1}$ by using Stirling's formula. Then, the corresponding α_0 is $-\Phi^{-1}((p + p^a)^{-1})$.

To make a comparison between the discrete SpSL prior and its neuronized version, we consider the Boston housing price data under the linear regression model in (1), which contains $n = 506$ median housing prices of owner-occupied homes in the Boston area, together with ten variables that might be associated with the median prices. Under the Jeffrey's prior on σ^2 , that is $1/\sigma^2$, we consider the independent neuronized prior that is $\theta_j = T(\alpha_j - \alpha_0)w_j$, where $\alpha_j \sim N(0, 1)$ and $w_j \sim N(0, \sigma^2 \tau_w^2)$ for $j = 1, \dots, p$. The solution path of each variable selection procedure is provided in Figure 2, and it shows that the solution path of the neuronized prior with the ReLU function T is almost identical to that of the standard discrete SpSL prior.

2.2 Bayesian Lasso

Bayesian Lasso imposes an double-exponential prior on θ_j and uses a latent-variable representation to facilitate efficient MCMC computations (Park & Casella 2008). We show below that with the identity activation function $T(t) = t$, the resulting neuronized prior is approximately equivalent to the Bayesian Lasso prior. The similarity between Bayesian Lasso and the neuronized prior under the identity activation function can be explained by the marginal density form of the neuronized prior demonstrated in the following lemma.

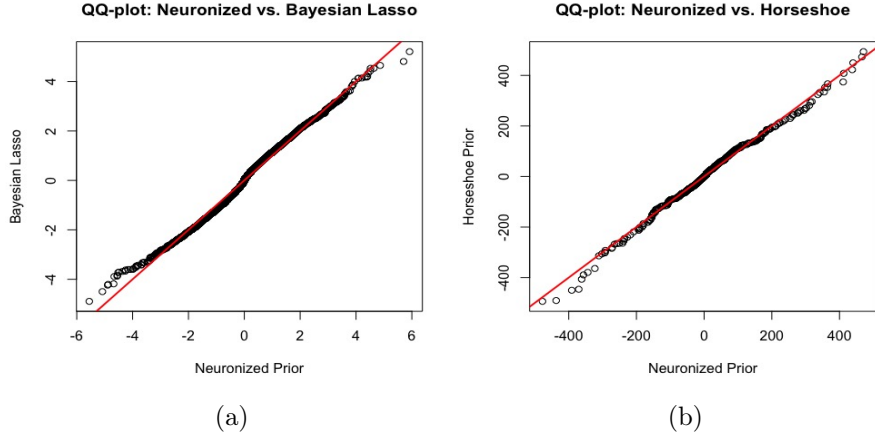


Figure 3: QQ plots of 100,000 samples from existing priors and their neuronized versions. The 45°sloped-line is plotted in red.

Lemma 2.1. *The use of an activation function $T(t) = t$ results in the marginal density θ of the neuronized prior being proportional to $\int_0^\infty z^{-1} \exp\{-\theta^2/(2\tau_w^2 z^2) - z^2/2\} dz$.*

The form under the integral is similar with that of the Bayesian Lasso prior, i.e., $\exp\{-|\theta|/\tau_w\} \propto \int_0^\infty \exp\{-\theta^2/(2z^2) - z^2/(2\tau_w^2)\} dz$, and the only difference is the term z^{-1} in the integrand. Furthermore, the following proposition shows the tail behavior of the neuronized prior.

Proposition 2.2. *Let π_L the marginal density function of θ defined in (4) with $T(t) = t$ and $\alpha_0 = 0$. Then, for any $0 < \epsilon < 1$, there exists θ_0 such that $c_1 \exp\{-(1+\epsilon)^{1/2}|\theta|/\tau_w\} \leq \pi_L(\theta) \leq c_2 \exp\{-(1-\epsilon)^{1/2}|\theta|/\tau_w\}$, if $\theta > \theta_0$, for some constants c_1 and c_2 .*

Proposition 2.2 shows that when T is linear, the resulting neuronized priors attain the same tail behavior as that of Bayesian Lasso (double exponential) prior. This result also suggests that the slab part in the neuronized prior based on the ReLU function also has an exponential tail. This tail behavior is theoretically desirable, because the adaptive minimax rate of the posterior contraction can be achieved when the tails of the slab part in the discrete SpSL prior are at least exponential (or heavier) (Castillo et al. 2012, 2015).

Figure 3(a) shows a QQ plot of 100,000 samples from the Bayesian Lasso prior and its neuronized version, verifying that the two distributions are indeed very similar. There exists, however, a small bump in the QQ plot, showing that the neuronized prior has

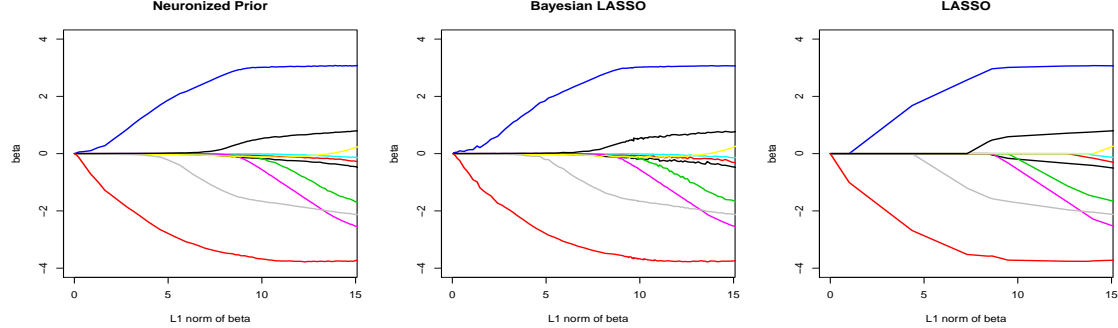


Figure 4: Solution paths of the neuronized prior, the Bayesian Lasso and the Lasso.

slightly more density around zero than the standard Bayesian Lasso prior. Figure 4 shows the solution paths of the Bayesian Lasso, the neuronized Bayesian Lasso, and the standard Lasso for the analysis of the Boston housing price data set, and the three solution paths are almost identical.

A similar formulation related to Bayesian Lasso was considered in Hoff (2017). He showed that the MAP estimator based on the product representation of the parameter (i.e., the neuronized prior) is identical to the standard Lasso. This fact justifies the use of the linear activation function to approximate the Bayesian Lasso prior density.

2.3 Horseshoe prior

We propose a class of activation functions that lead the corresponding neuronized prior to approximate the horseshoe prior.

Proposition 2.3. *Let π_E the marginal density function of θ defined in (4) with $T(t) = \exp(\lambda_1 \text{sgn}(t)t^2 + \lambda_2 t)$ and $\alpha_0 = 0$ for $0 < \lambda_1 \leq 1/2$ and $\lambda_2 > 0$. Then, there exists θ_0 such that $c_1(\log |\theta|)^{-1/2}|\theta|^{-1-\frac{1}{2\lambda_1}} \leq \pi_E(\theta) \leq c_2(\log |\theta|)^{-1/2}|\theta|^{-1-\frac{1}{2\lambda_1}}$, if $\theta > \theta_0$, where c_1 and c_2 are some constants, and $\text{sgn}(\cdot)$ is the sign function.*

Proposition 2.3 indicates that when $T(t) = \exp\{\lambda_1 \text{sgn}(t)t^2 + \lambda_2 t\}$ for some λ_1 and λ_2 , the tail behavior of the corresponding neuronized prior is polynomial. We numerically evaluated the neuronized prior that was closest to the horseshoe prior by choosing $T(t) = \exp\{0.37 \text{sgn}(t)t^2 + 0.89t + 0.08\}$. The details of a general numerical derivation are given in Section 3.1.

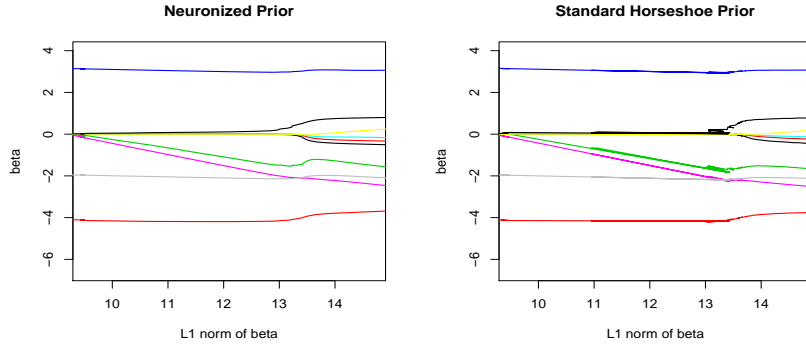


Figure 5: Solution paths of the neuronized prior and the horseshoe prior.

Figure 3(b) shows a QQ plot of 100,000 samples from the horseshoe prior against its neuronized version, illustrating that the two marginal prior distributions are very similar. Figure 5 compares the solution paths under the two priors for the same Boston housing price data, again demonstrating their nearly identical behaviors. Finally, we summarize the connections between the existing priors and the neuronized prior in Table 1.

Activation function T	Existing Prior
$T(t) = \max\{0, t\}$ (ReLU)	Discrete SpSL prior
$T(t) = t$ (linear)	Approximately Bayesian Lasso
$T(t) = \exp\{0.37\text{sgn}(t)t^2 + 0.89t + 0.08\}$	Approximately horseshoe prior

Table 1: The choice of T for neuronized priors and the corresponding existing Bayesian priors.

Although the neuronization formulation we introduced in (4) covers a large class of prior densities as demonstrated, it cannot approximate all possible priors. For example, nonlocal prior densities (Johnson & Rossell 2010, 2012, Rossell & Telesca 2017), which have bimodal shapes symmetric around zero, are not be formulated by the neuronized prior. However, it is still possible to capture the bimodality of a density by imposing a bimodal prior density on w for the neuronized prior, instead of the Gaussian. Also, dependent prior densities cannot be represented by the product of independent densities. These examples include the Zellner's g -prior (Zellner 1986) and the Dirichlet-Laplace prior (Bhattacharya et al. 2015). But an extension of the neuronized prior to a multivariate version may overcome this limitation.

Remark. When a linear activation function is used, the parameter itself $\theta_j (= \alpha_j w_j)$ is identifiable. However, there is an unidentifiability issue for individual α_j and w_j since switching signs of α_j and w_j induces the same parameter value, i.e., $(-\alpha_j)(-w_j) = \alpha_j w_j$. In contrast, for the ReLU activation function and the exponential activation function for the horseshoe prior, the α_j and w_j are identifiable because these activation functions are non-decreasing and their codomains are non-negative.

3 Managing the Neuronized Prior

3.1 Find the activation function to match a given prior

We have examined that some existing priors can be approximately represented by the neuronized priors as summarized in Table 1. However, it is still not clear how to choose the activation function T when we want to approximate a given arbitrary prior density. To address this issue, we propose a numerical procedure to derive an activation function T that leads the corresponding neuronized prior to match a given prior density, $\pi(\theta)$. We denote by T_ϕ the class of activation functions that may be used by a neuronized prior, where ϕ is a parameter that determines the form of the activation function. For example, B-spline basis functions can be used to approximate the activation function, which can be expressed as $T_\phi(t) = \mathbf{B}(t)\phi$, where \mathbf{B} is a vector of K B-spline basis functions and $\phi \in \mathbb{R}^K$.

We first draw a large number, S , of i.i.d. pairs $(\alpha_i, w_i) \sim N(0, 1) \times N(0, \tau_w^2)$ for $i = 1, \dots, S$, and then derive a sample of S i.i.d. draws from the neuronized prior as

$$\tilde{\theta}_{\phi,i} = T_\phi(\alpha_i - \alpha_0)w_i, \quad i = 1, \dots, S.$$

We also generate a sample of S i.i.d. draws from the original prior, $\theta_i \sim \pi(\theta)$ for $i = 1, \dots, S$. We measure the distance between these two samples, for example, by defining the distance $D(\phi) = \sum_{i=1}^S (\tilde{\theta}_{\phi,i}^{(i)} - \theta_i^{(i)})^2$, where $\tilde{\theta}_{\phi,i}^{(i)}$ and $\theta_i^{(i)}$ are the i -th order statistics of the generated samples $\{\tilde{\theta}_{\phi,i}\}_{i=1,\dots,S}$ and $\{\theta_i\}_{i=1,\dots,S}$, respectively. Some other attractive measures are the Kolmogorov-Smirnov or the Wasserstein distances. Then, we can minimize $D(\phi)$ with respect to ϕ by using a grid search algorithm or a simulated annealing algorithm (Kirkpatrick & Vecchi 1983). This optimization is not computationally intensive as long as the dimension of ϕ is moderate.

3.2 The choice of hyperparameters

Neuronized priors have two hyperparameters: the variance of the global shrinkage parameter τ_w^2 and the bias parameter α_0 . The roles of these hyperparameters are different according to the choice of the activation function. When a ReLU function is considered, the corresponding neuronized prior is equivalent to a discrete SpSL prior, and the sparsity level of the parameter is mainly determined by α_0 , i.e., the prior probability for each coefficient to be non-zero is $\Phi(-\alpha_0)$. One might consider a hyperprior on α_0 to avoid choosing the value. However, sampling α_0 in MCMC step is challenging, because there is no explicit form of the conditional posterior distribution of α_0 and the hyperparameter α_0 is highly correlated with α_j and w_j for $j = 1, \dots, p$ *a posteriori*.

When we consider the neuronized version of a continuous shrinkage prior, the shrinkage level of the parameter is controlled by the variance of the global shrinkage parameter τ_w^2 and we implicitly assume $\alpha_0 = 0$. As the τ_w^2 gets smaller, more prior density would concentrate around zero so that the resulting posterior distribution also attains more density around zero. Even though some asymptotic rate of the global shrinkage parameter was proposed to achieve the minimax optimal posterior contraction based on the horseshoe prior in van der Pas et al. (2014) under normal mean models, a practical selection of the hyperparameter is still unclear. For this, a hyperprior can be imposed on τ_w^2 . Gelman (2006) argued that the hyperprior on the variance parameter should have enough density around zero, and recommended the use of a half-Cauchy prior. However, half-Cauchy priors implicitly contain a scale hyperparameter, and the standard half-Cauchy prior density is a special case with the scale parameter one; i.e., $\pi(\tau_w^2) \propto (1 + a\tau_w^2)^{-1}$ for the scale parameter $a = 1$. Piironen & Vehtari (2017) provided some general examples where the posterior distribution of the regression coefficients is sensitive to the scale of the half-Cauchy prior. They concluded that the use of the standard half-Cauchy prior can lead to bad results and it is desirable to explicitly choose the global shrinkage parameter. In this sense, instead of imposing the standard Cauchy prior on the global shrinkage parameter, we set $\tau_w^2 = p^{-2}$ by following a theoretical rate investigated in van der Pas et al. (2014) for the optimal posterior contraction rate of Gaussian mean models using a horseshoe prior (by assuming that the prior guess of the number of the true variables is one). We subsequently use this setting and show that the empirical performance of the resulting procedure is promising in various simulation and real data examples.

For linear regression model (1), the scale of the parameter can be critical in discerning the signal from noise. Thus, it is desirable to scale the variance of w_j relative to σ^2 so that $w \sim N(0, \sigma^2 \tau_w^2)$. We do not consider this modification to the prior variance of α . One

reason is that a different scale of α affects the sparsity control. For a ReLU activation function, the prior probability of θ being zero is $\Phi(-\alpha_0/\sigma)$, when $\alpha \sim N(0, \sigma^2)$. Usually, the value of σ^2 is unknown so that the control of the prior sparsity level is almost impossible in this case. The other reason is that when σ^2 is multiplied to both variance of the scale and weight parameters, the scale of the original parameter θ can be inflated to σ^4 .

4 Sampling and Optimization with Neuronized Priors

In this section, we describe computational strategies for Bayesian linear regression inference with the neuronized priors including both MCMC algorithms for sampling from the posterior distribution and optimization algorithms to evaluate the MAP estimator.

4.1 MCMC sampling with neuronized priors

Consider the linear regression model in (1) and the independent neuronized prior (4) on each regression coefficient. The unnormalized form of the posterior distribution of α and w is expressible as

$$\pi(\boldsymbol{\alpha}, \mathbf{w} | \mathbf{y}, \sigma^2) \propto \exp \left\{ -\frac{\|\mathbf{y} - X\theta(\boldsymbol{\alpha}, \mathbf{w})\|_2^2}{2\sigma^2} - \frac{\boldsymbol{\alpha}^T \boldsymbol{\alpha}}{2} - \frac{\mathbf{w}^T \mathbf{w}}{2\sigma^2 \tau_w^2} \right\} \pi(\sigma^2), \quad (7)$$

where $\pi(\sigma^2)$ is the prior on σ^2 , $\boldsymbol{\alpha} = \{\alpha_1, \dots, \alpha_p\}^T$, $\mathbf{w} = \{w_1, \dots, w_p\}^T$, and $\theta(\boldsymbol{\alpha}, \mathbf{w}) = \{T(\alpha_1 - \alpha_0)w_1, \dots, T(\alpha_p - \alpha_0)w_p\}^T \equiv D_\alpha \mathbf{w}$, with D_α denoting the diagonal matrix of the $T(\alpha_j - \alpha_0)$'s.

The conditional posterior distribution of \mathbf{w} given $\boldsymbol{\alpha}$ and other hyperparameters is Gaussian, which can simplifies its sampling:

$$\mathbf{w} | \mathbf{y}, \boldsymbol{\alpha}, \sigma^2, \tau_w^2 \sim N(\tilde{\mu}, \sigma^2 \tilde{\Sigma}), \quad (8)$$

where $\tilde{\Sigma} = (D_\alpha X^T X D_\alpha + \tau_w^{-2} I)^{-1}$ and $\tilde{\mu} = \tilde{\Sigma} D_\alpha X^T \mathbf{y}$. When an inverse-gamma prior $\text{Inv-Gam}(a_0, b_0)$ is imposed on σ^2 , the Gibbs update of σ^2 follows $\text{Inv-Gam}((n+p)/2 + a_0, \|\mathbf{y} - X\theta\|_2^2/2 + \mathbf{w}^T \mathbf{w}/(2\tau_w^2) + b_0)$. When p is large relative to n , the numerical calculation of $(D_\alpha X^T X D_\alpha + \sigma^2 I)^{-1}$ is very expensive. Bhattacharya et al. (2016) proposed a fast sampling procedure that reduces the computational complexity from $O(p^3)$ to $O(n^2 p)$, which is employed here. Conditional on \mathbf{w} and $\boldsymbol{\alpha}_{(-j)}$, each α_j can be sampled by a naive random-walk Metropolis-Hastings (RWMH) algorithm, for $j = 1, \dots, p$. Since w_j and α_j

Algorithm 1 The MCMC algorithm for neuronized priors

For $i = 1, \dots, N$

- Sample \mathbf{w} conditional on $\mathbf{y}, \boldsymbol{\alpha}, \sigma^2$ from (8).
- Update $r = y - \mathbf{X}\boldsymbol{\theta}(\alpha, w)$.

For $j = 1, \dots, p$

- Set $r = r + X_j T(\alpha_j - \alpha_0) w_j$.

Repeat M times

- Sample α_j from $[\alpha_j \mid \mathbf{y}, \boldsymbol{\alpha}_{(-j)}, \mathbf{w}_{(-j)}, \sigma^2, \tau_w^2]$ by using a RWMH step for the log-target function $-\log(v_j)/2 - \alpha_j^2/2 + v_j m_j^2/(2\sigma^2)$, —(*) where $v_j = X_j^T X_j T^2(\alpha_j - \alpha_0) + 1/\tau_w^2$ and $m_j = r_j^T X_j T(\alpha_j - \alpha_0)/v_j$.
- Sample w_j from $[w_j \mid \mathbf{y}, \boldsymbol{\alpha}_{(-j)}, \alpha_j, \mathbf{w}_{(-j)}, \sigma^2, \tau_w^2]$, which is $N(m_j, \sigma^2 v_j^{-1})$.

End.

- Update $r = r - X_j T(\alpha_j - \alpha_0) w_j$.

End.

- Sample σ^2 from $[\sigma^2 \mid \mathbf{y}, \boldsymbol{\alpha}, \mathbf{w}, \tau_w^2]$, which is an inverse Gamma.

End.

tend to be highly correlated *a posteriori*, a better strategy is to integrate out w_j so as to draw α_j^* from $\pi(\alpha_j \mid \mathbf{y}, \mathbf{w}_{(-j)}, \boldsymbol{\alpha}_{(-j)})$, and then draw w_j from $\pi(w_j \mid \mathbf{y}, \mathbf{w}_{(-j)}, \boldsymbol{\alpha}_{(-j)}, \alpha_j^*)$.

The RWMH step in Algorithm 1 is rather local and cheap; we typically iterate the RWMH step M times. We used $M = 10$ in all our numerical examples, and found the resulting algorithm to perform well. We use a Gaussian distribution with standard deviation 2 as the proposal distribution, which enables α_j to jump efficiently between the regions $\{\alpha_j : \alpha_j < \alpha_0\}$ and $\{\alpha_j : \alpha_j \geq \alpha_0\}$. We subsequently use Algorithm 1 as the default to implement the posterior inference based on the neuronized prior.

4.2 Properties of the ReLU activation function in MCMC

A most direct and effective approach for conducting sparse Bayesian linear regression is to employ a discrete SpSL prior for the coefficients. When the continuous component of this prior is conjugate to the Gaussian likelihood, one of the best known computational strategies is to integrate out all the continuous parameters (e.g., regression coefficients and the variance parameter) and to sample directly the binary indicator vector $\boldsymbol{\gamma}$ in (3) from

its posterior distribution by MCMC. This posterior distribution can be defined as

$$\pi(\boldsymbol{\gamma} | \mathbf{y}) = \frac{m_{\boldsymbol{\gamma}}(\mathbf{y})g(\boldsymbol{\gamma})}{\sum_{\boldsymbol{\gamma}'} m_{\boldsymbol{\gamma}'}(\mathbf{y})g(\boldsymbol{\gamma}')}, \quad (9)$$

where $m_{\boldsymbol{\gamma}}(\mathbf{y})$ is the marginal likelihood of $\boldsymbol{\gamma}$ and $g(\cdot)$ is the model prior. Since the number of possible $\boldsymbol{\gamma}$ increases exponentially in p , a naive RWMH algorithm on the discrete posterior model space can become very inefficient under high-dimensional settings. Moreover, in every MCMC iteration, one has to calculate the marginal likelihood of the current model, which requires a matrix inversion step. Even though the size of the matrix to be inverted should be much smaller than p under sparsity settings, multiple evaluations of the matrix inversion at every iteration significantly slow down the computation. Furthermore, even this approach is unavailable if one cannot analytically integrate out the continuous parameters. In such cases, either a crude approximation strategy, or a clever and specially designed yet case-specific data augmentation scheme (Polson et al. 2013), or a much less efficient reversible-jump scheme (Green 1995) has to be employed.

In contrast, our neuronized prior with ReLU activation can achieve the same effect as using the discrete SpSL prior and give rise to more efficient computation, even if one cannot integrate out the continuous component in the joint posterior distribution. In Sections 5 and 6, we show with numerical examples how this procedure improves the sampling efficiency compared to the best-available MCMC procedure based on the conjugate discrete SpSL.

When a ReLU activation function is adopted, the posterior space becomes non-smooth with respect to $\boldsymbol{\alpha}$. As a result, the efficiency of RWMH sampling for α_j might be compromised. We show below that conditional distribution $\pi(\alpha_j | \mathbf{y}, \mathbf{w}_{(-j)}, \boldsymbol{\alpha}_{(-j)})$ is a mixture of two truncated Gaussians, which can be sampled exactly so as to avoid some inefficient RWMH steps.

Proposition 4.1. *Let $\boldsymbol{\alpha} = (\alpha_1, \dots, \alpha_p)$, and let $\boldsymbol{\alpha}_{(-j)}$ denote the corresponding vector excluding the j -th component α_j . We denote a truncated Gaussian distribution with mean a and variance b on (c, d) by $N_{tr}(a, b; c, d)$. Suppose that the full posterior distribution based on the neuronized prior is expressible as (7) and a ReLU function is used as the activation function. Then, $\alpha_j | \boldsymbol{\alpha}_{(-j)}, \mathbf{w}, \mathbf{y}, \sigma^2 \sim \kappa N_{tr}(0, 1; -\infty, \alpha_0) + (1 - \kappa) N_{tr}(\tilde{\alpha}_j, \tilde{\sigma}_j^2; \alpha_0, \infty)$, where $\tilde{\alpha}_j = (r_j + X_j \alpha_0 w_j)^T X_j w_j / (X_j^T X_j w_j^2 + \sigma^2)$, $\tilde{\sigma}_j^2 = \sigma^2 (X_j^T X_j w_j^2 + \sigma^2)^{-1}$, and*

$$\kappa = \frac{\Phi(\alpha_0) \exp \left\{ -\frac{\|r_j\|_2^2}{2\sigma^2} \right\}}{\Phi(\alpha_0) \exp \left\{ -\frac{\|r_j\|_2^2}{2\sigma^2} \right\} + \left\{ 1 - \Phi \left(\frac{\alpha_0 - \tilde{\alpha}_j}{\tilde{\sigma}_j} \right) \right\} \tilde{\sigma}_j \exp \left\{ \frac{\tilde{\alpha}_j^2}{2\tilde{\sigma}_j^2} - \frac{\|r_j + X_j \alpha_0 w_j\|_2^2}{2\sigma^2} \right\}}.$$

There is the other computational advantage of using the ReLU activation function. When sampling \mathbf{w} in a Gibbs step, the conditional posterior distribution can be decomposed as a product of some independent Gaussian densities so that it avoids the numerical inversion of the $p \times p$ matrix $\tilde{\Sigma}$ in (8). Note that the mean vector $\tilde{\mu}$ and the covariance matrix $\tilde{\Sigma}$ in (8) can be expressed as

$$\tilde{\Sigma} = \begin{pmatrix} D_\alpha^* X^{*\top} X^* D_\alpha^* + \tau_w^{-2} \mathbf{I} & 0 \\ 0 & \tau_w^{-2} \mathbf{I} \end{pmatrix}, \quad \tilde{\mu} = \begin{pmatrix} (D_\alpha^* X^{*\top} X^* D_\alpha^* + \tau_w^{-2} \mathbf{I})^{-1} D_\alpha^* X^{*\top} \mathbf{y} \\ 0 \end{pmatrix},$$

where D_α^* and X^* are the sub-matrices induced by the index of the nonzero regression coefficients. This expression means that for j such that $\alpha_j < \alpha_0$, the corresponding coefficient θ_j is set to zero and the sampling of w_j follows an independent Gaussian distribution $N(0, \sigma^2 \tau_w^2)$. The conditional distribution of the sub-vector $\mathbf{w}^* = \{w_j : \alpha_j > \alpha_0\}$ is then $N(\tilde{\mu}^*, \sigma^2 \tilde{\Sigma}^*)$, where $\tilde{\Sigma}^* = D_\alpha^* X^{*\top} X^* D_\alpha^* + \tau_w^{-2} \mathbf{I}$ and $\tilde{\mu}^* = \tilde{\Sigma}^{*-1} D_\alpha^* X^{*\top} \mathbf{y}$. To sample \mathbf{w}^* , we only need to invert $D_\alpha^* X^{*\top} X^* D_\alpha^* + \tau_w^{-2} \mathbf{I}$, which has a much smaller size than the $p \times p$ matrix $\tilde{\Sigma}$. The computational complexity of this step is only $O(|\mathbf{w}^*|^3) + O(p - |\mathbf{w}^*|) + O(n|\mathbf{w}^*|)$, where $|\mathbf{w}^*|$ is the number of elements in \mathbf{w}^* , while the computational complexity of the original form is $O(p^3) + O(np)$.

4.3 A scalable algorithm for finding posterior mode

For massive-sized data sets, MCMC algorithms may be prohibitively slow, so we may need to consider optimization-based algorithms for obtaining the MAP estimator. We here propose a coordinate-ascent algorithm to evaluate the MAP estimator. The proposed algorithm adopts a warm start procedure, which begins with a hyperparameter resulting in a weak shrinkage and gradually increases the strength of the shrinkage. This warm start idea has also been adopted by Rockova & George (2018) for finding the MAP estimator using an EM algorithm. While this warm start technique requires multiple implementations of the optimization with various hyperparameters so that the total computational burden is heavier than a single optimization, the proposed approach alleviates the danger of being trapped in a local optimum. Although the proposed algorithm is not theoretically free of the local optima issue, our empirical results from both simulation studies and real data examples in Sections 5 and 6 show that the algorithm performed significantly better than existing methods. The detailed algorithm is described in Algorithm 2.

A key to the success of this algorithm depends on the optimization with respect to α_j while fixing other parameters such as $\boldsymbol{\alpha}_{(-j)}$ and \mathbf{w} . The vector \mathbf{w} is updated jointly conditioning on $\boldsymbol{\alpha}$ by taking advantage of the Gaussian conjugacy. Because the function

of α_j in (•) of Algorithm 2 is a linear combination of a quadratic function and a function of $T(\alpha_j - \alpha_0)$, we divide the optimization space into two parts ($\{\alpha_j : \alpha_j > \alpha_0\}$ and $\{\alpha_j : \alpha_j \leq \alpha_0\}$), and find a local maximum from each part. Then, we update α_j to the local maximum that has a larger objective value. This is an one-dimensional optimization problem, and a local maximum can be easily found by existing optimization algorithms such as secant algorithms (Brent 1973, Dekker 1969), constrained Newton-Raphson algorithms (Fischer 1992), constrained gradient descent algorithms (Tseng & Yun 2009), etc. In this article, we use the secant algorithm proposed by Brent (1973).

Algorithm 2 The coordinate-ascent algorithm for neuronized priors

- Initialize the parameters α , w , σ^2 , τ_w^2 .
- Set a candidate set of hyperparameters λ , $\{\lambda^{(1)}, \dots, \lambda^{(L)}\}$.

For $l = 1, \dots, L$

- Set $\alpha_0 = \lambda^{(l)}$ (or set $\tau_w = \lambda^{(l)}$).
- Set $r = y - X\theta(\alpha, w)$.

Until convergence

For $j = 1, \dots, p$

- Update $r = r + X_j T(\alpha_j - \alpha_0) w_j$.
- Update α_j by optimizing the logarithm of the marginalized posterior density function $-\log(v_j)/2 - \alpha_j^2/2 + v_j m_j^2/(2\sigma^2)$ with respect to α_j , where $v_j = X_j^T X_j T^2(\alpha_j - \alpha_0) + 1/\tau_w^2$ and $m_j = r_j^T X_j T(\alpha_j - \alpha_0)/v_j$. — (•)
- Update w_j by m_j .
- Update $r = r - X_j T(\alpha_j - \alpha_0) w_j$.

End.

End.

End.

For the ReLU activation function, α_0 crucially affects the sparsity level by the prior non-zero probability $\Phi(-\alpha_0)$ for each parameter, while the global shrinkage parameter τ_w^2 controls how much density is concentrated around zero for the neuronized version of continuous shrinkage priors. In the warm start procedure for the ReLU activation function, we start with $\alpha_0 = 0$ so that the prior probability that a regression coefficient is non-zero is $1/2$, and evaluate the MAP estimator. The resulting MAP estimator is then used as an initial value for the next step of optimization with a slightly increased α_0 . By doing so, we gradually increase α_0 until we reach the desired hyperparameter. In the simulation and real

data examples, we use the hyperparameter schedule that is a equi-spaced sequence between 0 and the target hyperparameter with size 20. For the neuronized version of continuous shrinkage priors, the hyperparameter controlled in the warm start procedure is the global shrinkage parameter τ_w^2 . We typically start with a large τ_w^2 , such as 1, and then decrease τ_w^2 gradually to a certain value. The hyperparameter schedule used in the following examples is p^{C_τ} , where C_τ is a equi-spaced sequence between 0 and $(\log \tau_{w0}^2) / \log p$ with size 20, and τ_{w0}^2 is the target hyperparameter.

Throughout the optimization algorithm, the error variance σ^2 is fixed, in advance, at the MLE using the top variables selected from all candidate ones based on marginal correlations (no more than $0.1 \times n$). We do not update σ^2 in the algorithm because in the posterior space the regression coefficients are highly correlated with σ^2 so that the optimization is more likely trapped in a local maximum. The results in the following sections show that this procedure works well for various real and simulated data sets.

4.4 Comparisons with other posterior optimization procedures

Yen et al. (2011) proposed a MM algorithm to find the MAP estimator of discrete SpSL priors by approximating l_0 norm by a log-transformed function. By following the notation used in the article, the approximation is $\|\theta\|_0 = \lim_{\tau_3 \rightarrow 0} \sum_{j=1}^p \log(1 + \tau_3^{-1} |\theta_j|) / (\log(1 + \tau_3^{-1}))$. In practice, however, we need to fix the hyperparameter τ_3 in advance, and the performance of the approximation is crucially determined by the choice of τ_3 . While a smaller τ_3 results in a better approximation to the original posterior distribution, the resulting target function becomes highly non-concave and is much more difficult to optimize.

EMVS (Rockova & George 2014) and SSLasso (Rockova & George 2018) were proposed to evaluate the MAP estimator of a continuous SpSL prior in (3) based on an EM formulation. The prior for the EMVS is a mixture of two Gaussian densities, $\pi_0 = N(0, \nu_0)$ and $\pi_1 = N(0, \nu_1)$, and that for the SSLasso is a mixture of two Laplace densities, $\pi_0 = \text{Laplace}(\lambda_0)$ and $\pi_1 = \text{Laplace}(\lambda_1)$, where $\nu_0 \ll \nu_1$ and $\lambda_0 \gg \lambda_1$. It can mimic a point mass mixture of a sparsity-inducing prior by setting the variance of π_0 to be very small. Since the spike prior part is not a point mass (but a continuous prior), an extra hyperparameter ν_0 (or λ_0) needs to be chosen to control how much the spike prior density is concentrated around zero. To make a computational comparison with the neuronized MAP estimator evaluated by Algorithm 2, we set $\eta = p^{-1}$ in (5); and then choose $\nu_1 = 10$ and $\nu_0 = 10^{-3}$ for the EMVS, and choose $\lambda_1 = 0.1$ and $\lambda_0 = 1000$ for SSLasso.

Figure 6 shows a comparison of optimization paths of the MM algorithm, the EMVS, the SSLasso, and Algorithm 2 for the variable selection procedure of the Bardet-Biedl data

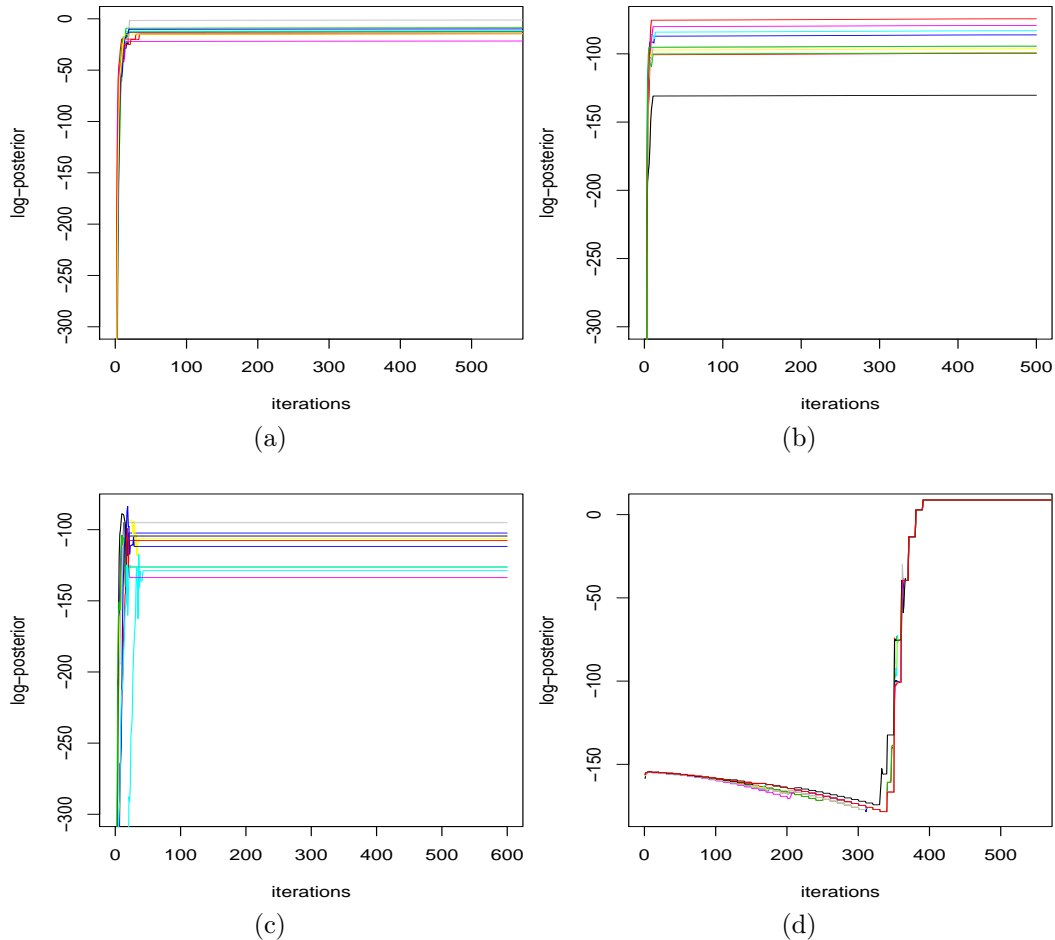


Figure 6: Trace plots of the optimization algorithms from 10 different initial points: (a) MM with $\tau_3 = 10^{-2}$; (b) EMVS; (c) SSLasso; (d) Neuronized prior by Algorithm 2.

set ($n = 120$ and $p = 200$), which will be discussed in more details in Section 6. Each different colored-line indicates an optimization path based on a randomly generated initial point. As shown in Figure 6, the other optimization-based procedures obviously failed to find the high posterior region, and the solutions were very sensitive to the initial point – ten randomly selected initial points resulted in ten different solutions in our example. In contrast, Algorithm 2 for the neuronized prior found the same MAP estimator from different initial points. In Section 5 and Section 6, we provide a more thorough performance comparison of aforementioned optimization algorithms: MM, EMVS, SSLasso, and Algorithm 2, for various synthetic and real data sets.

To reduce the risk of trapping in local maxima, we applied the warm start procedure to the MM algorithm and the SSLasso by gradually decreasing (or increasing) its hyper-parameter; η for the MM algorithm and λ_0 for the SSLasso. Also, by following a recommendation of Rockova & George (2014), we used a deterministic annealing procedure to the EMVS to mitigate the issue of trapping in local maximum modes. Nevertheless, the optimized solutions by the MM algorithm, the EMVS, and the SSLasso are still sensitive to different initial points.

5 Simulation Studies

In this section, we examine how neuronized priors perform for synthetic data sets under both low-dimensional and high-dimensional settings. Under the Bayesian regression framework, we compare effects of some standard priors such as the Bayesian Lasso prior, the horseshoe prior, and the discrete SpSL prior in (5) with those of their corresponding neuronized versions. In this simulation study, we also consider penalized two likelihood procedures: Lasso (Tibshirani 1996) and *Smoothly Clipped Absolute Deviation Penalty* (SCAD) (Fan & Li 2001).

5.1 Simulation setups and evaluation criteria

We examine two covariance structures to generate the predictors: (i) Independent covariates: $X_i \sim N(0, I)$, $i = 1, \dots, n$, where I is the $p \times p$ identity matrix; (ii) AR(1) dependent structure: for $X_i \sim N(0, \Sigma)$, $i = 1, \dots, n$, where $\sigma_{lk} = 1$, if $k = l$ and $\sigma_{lk} = 0.7^{|l-k|}$, otherwise for $1 \leq l, k \leq p$. For the low-dimensional cases, we test two settings of the sample size and the total number of predictor variables: (i) $n = 100, p = 50$; and (ii) $n = 400, p = 100$. The number of nonzero regression coefficients is 10% of p , and the regression coefficients are equally set to be s with random signs. We use $s = 0.3$ and $s = 0.2$ to examine strong signal

and weak signal scenarios, respectively. For high-dimensional settings, we fix the regression coefficients at $\beta_0 = s \times \{0.4, 0.45, 0.5, 0.55, 0.6, 0, \dots, 0\}$ for $s = 1$ and $s = 1.5$ under two settings: (iii) $n = 100, p = 300$; and (iv) $n = 150, p = 1000$. The sign of each coefficient is randomly assigned. We set the true error variance to be $\sigma^2 = 1$ for all scenarios.

We choose the tuning parameter of Lasso and SCAD by using cross-validation. Alternatively, we also consider Bayesian Information Criterion (BIC) for low dimensional settings and Extended BIC (EBIC, (Chen & Chen 2008)) for high-dimensional settings to select the tuning parameter. The EBIC can be written as $\text{EBIC}(\mathbf{k}) = \text{BIC} + \zeta |\mathbf{k}| \log p$, where \mathbf{k} denote the set of selected variables, $|\mathbf{k}|$ is the cardinality of \mathbf{k} and ζ is a tuning parameter. By following a default setting in Chen & Chen (2008), we set $\zeta = 1$.

We evaluate the ability of Algorithm 2 in finding the the MAP estimator of our neuronized version of (5) (denoted as N-SpSL(MAP)) and compare it to MM, EMVS and SSLasso. In this simulation study, we first fix $\eta = p^{-1}$ in (5), and $\nu_1 = 10$ for the EMVS and $\lambda_1 = 0.1$ for SSLasso. Then, we evaluate the MAP estimators based on different choices of ν_0 for the EMVS and λ_0 for the SSLasso, and select a value that minimizes the information criterion (BIC for low-dimensions and EBIC for high-dimensions). To implement these procedures, we use R packages EMVS and SSLasso (available on the CRAN or <http://faculty.chicagobooth.edu/veronika.rockova/>).

To evaluate the estimation performance of the neuronized priors, we report the *Mean Squared Error* (MSE) and the angle between the true regression coefficient and the estimated coefficients by each method. More precisely, the angle is defined as $\theta_0^T \hat{\theta} / \{(\theta_0^T \theta_0)^{1/2} (\hat{\theta}^T \hat{\theta})^{1/2}\}$, where θ_0 is the true regression coefficient and $\hat{\theta}$ is the estimated coefficient. The angle measure is more stringent as it cannot benefit from a simple shrinkage. To measure model selection performances, we examine the *Matthews correlation coefficient* (MCC; Matthews (1975)) defined as, $\text{MCC} = (\text{TP} \cdot \text{TN} - \text{FP} \cdot \text{FN}) / \{(\text{TP} + \text{FP})(\text{TP} + \text{FN})(\text{TN} + \text{FP})(\text{TN} + \text{FN})\}$, where TP, TN, FP, and FN denote the number of true positives, true negatives, false positives, and false negatives, respectively. MCC is generally regarded as a balanced measure of variable selection procedures that simultaneously takes into account TP, TN, FP, and FN. The value of MCC is bounded by one, and the closer to one MCC is, the better a model selection procedure is.

We consider the *Effective Sample Size* (ESS) to measure the efficiency of a MCMC procedure, which is defined as $\text{ESS} = N / (1 + 2 \sum_t^\infty \rho(t))$, where N is number of MCMC samples and $\rho(t)$ is the lag- t autocorrelation. To make comparisons across different Bayesian procedures, we report ESS per second, which is obtained from the R package coda.

5.2 Technical descriptions about computational strategies

For neuronized priors, we consider a RWMH step to sample α_j in Algorithm 1, and this setting is denoted by “RW” in parenthesis in the tables. For the neuronized version of the discrete SpSL prior via a ReLU activation function, we additionally consider a computational strategy that samples α_j from its exact conditional density in Proposition 4.1, denoted by “Exact” in parenthesis in the tables. We also evaluate the MAP estimator of the neuronized prior by using Algorithm 2, denoted by “MAP” in parenthesis. We examine the MM algorithm (Yen et al. 2011) for finding the MAP estimator with the discrete SpSL prior, in which two tuning parameters are tested: $\tau_3 = 10^{-2}$ and $\tau_3 = 10^{-6}$, denoted by “MM1” and “MM2” respectively in parenthesis. We do not consider the MAP estimator of the horseshoe prior nor its neuronized version. This is because as discussed in Carvalho et al. (2010) the individual marginal density of the horseshoe prior is infinite at zero, so the resulting MAP estimator is always the null value.

For Bayesian procedures based on SpSL priors in (3), we fix $\eta = p^{-1}$. Its neuronized version uses the ReLU activation function with $\alpha_0 = -\Phi^{-1}(p^{-1})$. We impose a prior on σ^2 proportional to $1/\sigma^2$ for all Bayesian procedures. For the horseshoe prior and its neuronized version, we fix the global shrinkage parameter as $\tau_w^2 = p^{-2}$, which is a theoretical rate investigated in van der Pas et al. (2014) for optimal posterior contraction for Gaussian mean models. For the Bayesian Lasso and its neuronized version, we choose the global shrinkage parameter that matches the tuning parameter value λ_{CV} determined by cross-validation for the standard Lasso procedure. This connection stems from the relationship between the Bayesian Lasso and the standard Lasso. That is, $\tau_w^2 = 2\hat{\sigma}_{CV}^2/\lambda_{CV}^2$, where $\hat{\sigma}_{CV}^2 = \|y - X\hat{\theta}_{\lambda_{CV}}\|_2^2/n$ with the Lasso estimator $\hat{\theta}_{\lambda_{CV}}$ based on tuning parameter λ_{CV} .

For the discrete SpSL prior, we use a Gaussian distribution for the slab part and a point mass at zero for the spike part. We also note that the use of a Gaussian prior in the slab part does not match the neuronized prior with the ReLU activation function since the product of two independent Gaussian random variables in the neuronization formulation results in a Laplace-like slab part. Nevertheless, we use the Gaussian slab prior to sustain computational efficiency by the Gaussian conjugacy. Due to the Gaussian conjugacy, the marginal likelihood of each model has a closed form, so it is not required to consider computationally more demanding approximation algorithm to evaluate the marginal likelihood. We note that the parameter estimation is mainly affected by the prior inclusion probability that is controlled by η in (5) and α_0 for the neuronized prior.

For the standard discrete SpSL prior, the MCMC algorithm works on the variable selection indicator space, i.e., the space of γ . We let the algorithm have a certain probability,

0.7 in our simulation studies, to propose a single flip move (i.e., randomly selecting a predictor, say predictor j , and propose to change its inclusion indicator γ_j to $1 - \gamma_j$), and 0.3 to propose a double-flip move. The proposed indicator vector γ' is accepted with probability $R(\gamma' | \gamma) = \min \{1, \pi(\gamma' | \mathbf{y})/\pi(\gamma | \mathbf{y})\}$, where $\pi(\gamma | \mathbf{y})$ is defined in (9). Given γ , by using the Gaussian conjugacy we can sample θ_γ easily. This MCMC algorithm for Bayesian variable selection has been used by numerous researchers (Madigan et al. 1995, Raftery et al. 1997, Brown et al. 1998, Guan & Stephens 2011), and its theoretical properties including the convergence rate of the MCMC chain has been investigated in Yang et al. (2016).

For the Gibbs sampler with Bayesian Lasso, the local shrinkage parameter can be sampled exactly from its conditional distribution, which is an inverse Gaussian distribution. For the Bayesian computation with the horseshoe prior, we use a slice sampler to sample each local shrinkage parameter. For both procedures, since the posterior distribution cannot provide a sparse solution directly, variables are selected by a hard thresholding step on the posterior mean of the regression coefficients. The threshold is set to be $0.1 \times \hat{\sigma}$, where $\hat{\sigma}^2$ is the posterior mean of σ^2 .

For all except the case with the discrete SpSL prior, we generate 20,000 MCMC samples after 2,000 burn-in iterations. For the discrete SpSL prior case, we simulate 200,000 MCMC samples because the acceptance rate of the RWMH algorithm for the standard procedure is very low (less than 2%). For all simulation scenarios, we replicate 100 data sets and average the results over the replications. All computations for MCMC algorithms are coded in C++ and implemented on a Xeon Broadwell processor with 16 cores of 1.8Ghz and 128GB RAM.

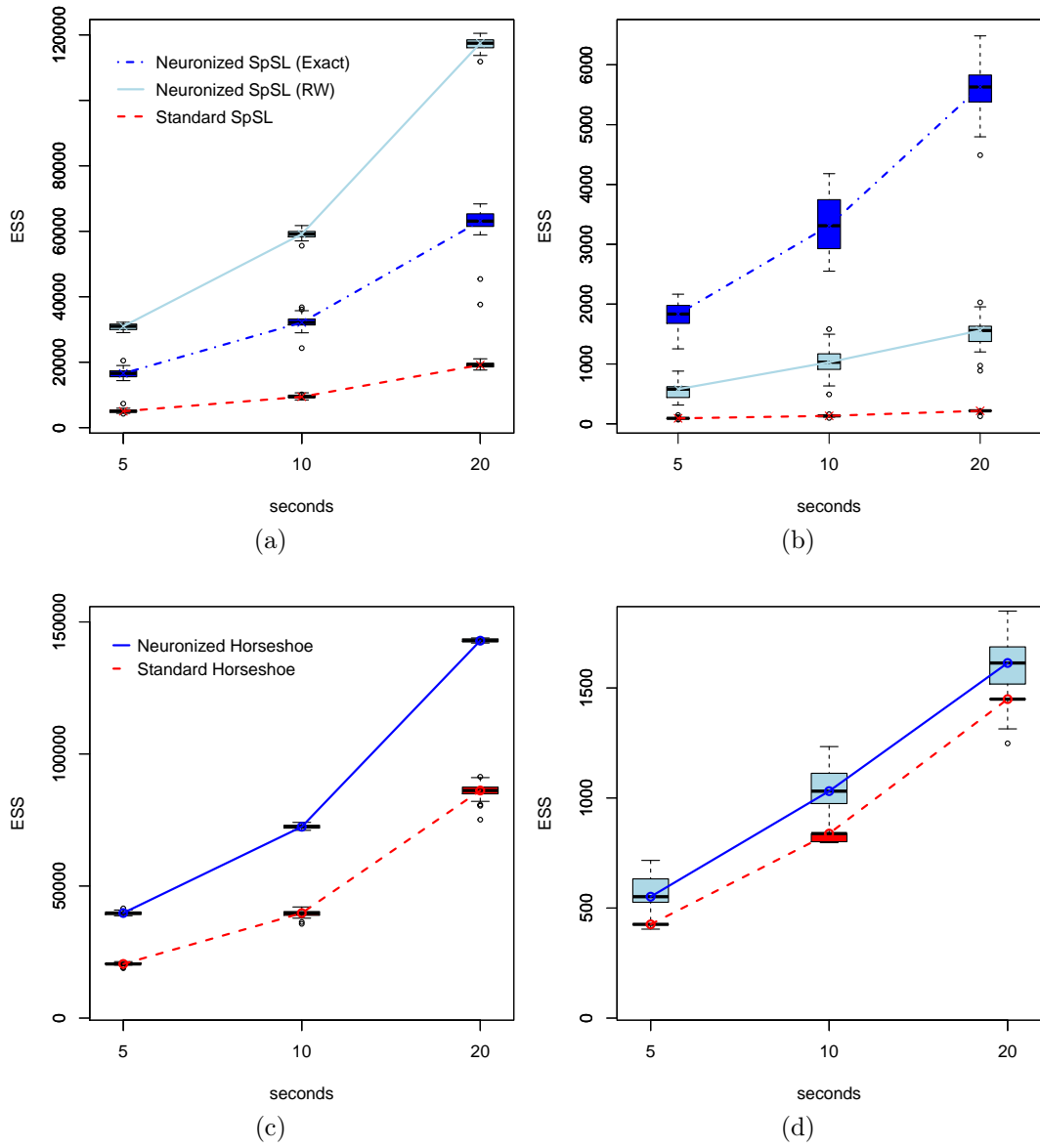


Figure 7: Effective samples size versus actual computation time for the Boston housing data set (the first column) and the Bardet-Biedl data set (the second column).

Method	Weak Signal ($s = 0.2$)									
	(n = 200, p = 50)					(n = 400, p = 100)				
	MSE	Angle	MCC	FP	ESS	MSE	Angle	MCC	FP	ESS
SpSL	0.129	0.619	0.52	0.05	88.1	0.174	0.754	0.70	0.00	26.8
SpSL(MM1)	0.111	0.759	0.67	2.45		0.125	0.853	0.72	6.06	
SpSL(MM2)	0.291	0.622	0.20	30.46		0.281	0.756	0.21	60.46	
N-SpSL(Exact)	0.127	0.621	0.49	0.03	5263.6	0.177	0.753	0.67	0.00	1260.8
N-SpSL(RW)	0.126	0.622	0.49	0.03	1374.0	0.177	0.753	0.67	0.00	376.8
N-SpSL(MAP)	0.111	0.697	0.67	0.67		0.080	0.898	0.89	0.91	
EMVS	0.187	0.670	0.46	6.34		0.260	0.751	0.37	26.41	
SSLasso	0.122	0.681	0.64	1.88		0.166	0.845	0.82	3.22	
HS	0.092	0.744	0.60	0.24	157.3	0.095	0.879	0.81	0.08	46.6
N-HS(RW)	0.092	0.742	0.60	0.24	623.2	0.095	0.878	0.81	0.09	176.5
BL	0.128	0.684	0.65	1.97	1235.9	0.140	0.817	0.87	1.03	360.3
N-BL(RW)	0.101	0.721	0.64	0.69	731.9	0.112	0.853	0.84	0.32	212.3
N-BL(MAP)	0.104	0.739	0.66	2.30		0.109	0.861	0.87	1.47	
Lasso(CV)	0.096	0.741	0.51	8.65		0.097	0.883	0.51	20.96	
SCAD(CV)	0.104	0.728	0.55	6.45		0.088	0.892	0.54	17.72	
Lasso(BIC)	0.146	0.619	0.68	0.93		0.202	0.812	0.86	1.64	
SCAD(BIC)	0.145	0.621	0.68	0.98		0.202	0.802	0.86	1.60	
Method	Strong Signal ($s = 0.3$)									
	(n = 200, p = 50)					(n = 400, p = 100)				
	MSE	Angle	MCC	FP	ESS	MSE	Angle	MCC	FP	ESS
SpSL	0.095	0.896	0.87	0.04	97.7	0.038	0.980	0.99	0.03	29.5
SpSL(MM1)	0.099	0.905	0.76	3.16		0.112	0.939	0.78	5.31	
SpSL(MM2)	0.282	0.782	0.22	29.54		0.289	0.866	0.22	60.14	
N-SpSL(Exact)	0.112	0.877	0.83	0.02	4236.1	0.046	0.976	0.99	0.03	1647.3
N-SpSL(RW)	0.112	0.878	0.83	0.02	1248.1	0.046	0.976	0.99	0.03	546.3
N-SpSL(MAP)	0.060	0.937	0.91	0.67		0.041	0.978	0.97	0.67	
EMVS	0.174	0.830	0.63	3.90		0.246	0.871	0.55	12.87	
SSLasso	0.151	0.890	0.85	1.76		0.155	0.923	0.87	2.91	
HS	0.076	0.919	0.92	0.25	161.2	0.051	0.973	0.99	0.09	50.5
N-HS(RW)	0.076	0.919	0.92	0.24	630.6	0.051	0.974	0.99	0.09	217.4
BL	0.141	0.841	0.79	2.68	1313.0	0.145	0.918	0.96	0.76	360.6
N-BL(RW)	0.105	0.881	0.90	0.72	753.2	0.107	0.945	0.99	0.19	239.1
N-BL(MAP)	0.107	0.881	0.78	2.94		0.106	0.942	0.94	1.34	
Lasso(CV)	0.091	0.906	0.52	10.70		0.095	0.958	0.53	19.72	
SCAD(CV)	0.080	0.920	0.55	8.94		0.049	0.974	0.63	12.47	
Lasso(BIC)	0.216	0.852	0.90	0.94		0.339	0.904	0.95	1.10	
SCAD(BIC)	0.211	0.847	0.89	0.99		0.306	0.896	0.94	1.21	

Table 2: Results for the low-dimensional setting with independent covariates. “SpSL”, “HS”, and “BL” indicate the procedure based on the discrete SpSL prior, the horseshoe prior, and the Bayesian Lasso prior, respectively. The sign “N” in front of each procedure means that it is a neuronized version of the corresponding prior.

Method	Weak Signal ($s = 0.2$)									
	(n = 200, p = 50)					(n = 400, p = 100)				
	MSE	Angle	MCC	FP	ESS	MSE	Angle	MCC	FP	ESS
SpSL	0.185	0.554	0.48	0.05	72.6	0.325	0.545	0.48	0.00	24.1
SpSL(MM1)	0.193	0.481	0.41	1.27		0.310	0.582	0.48	2.77	
SpSL(MM2)	0.550	0.470	0.20	22.26		0.616	0.579	0.21	46.19	
N-SpSL(Exact)	0.172	0.558	0.46	0.04	6015.4	0.316	0.541	0.46	0.00	1629.1
N-SpSL(RW)	0.173	0.555	0.46	0.04	1604.2	0.316	0.542	0.47	0.00	493.5
N-SpSL(MAP)	0.189	0.539	0.49	0.68		0.287	0.625	0.59	0.93	
EMVS	0.419	0.510	0.34	7.13		0.491	0.597	0.32	17.27	
SSLasso	0.201	0.470	0.46	1.11		0.364	0.485	0.48	2.20	
HS	0.131	0.645	0.54	0.12	154.6	0.248	0.648	0.55	0.02	47.8
N-HS(RW)	0.131	0.645	0.54	0.12	690.7	0.248	0.647	0.55	0.02	209.3
BL	0.164	0.616	0.53	2.04	1164.5	0.231	0.686	0.62	1.68	325.6
N-BL(RW)	0.129	0.660	0.55	0.99	765.5	0.213	0.695	0.60	0.43	239.8
N-BL(MAP)	0.152	0.616	0.54	1.70		0.226	0.684	0.61	1.86	
Lasso(CV)	0.134	0.608	0.48	5.34		0.228	0.668	0.45	13.61	
SCAD(CV)	0.222	0.528	0.39	3.72		0.339	0.572	0.38	8.86	
Lasso(BIC)	0.174	0.465	0.48	0.44		0.307	0.516	0.57	0.56	
SCAD(BIC)	0.187	0.465	0.45	0.69		0.361	0.475	0.50	1.14	
Method	Strong Signal ($s = 0.3$)									
	(n = 200, p = 50)					(n = 400, p = 100)				
	MSE	Angle	MCC	FP	ESS	MSE	Angle	MCC	FP	ESS
SpSL	0.337	0.608	0.54	0.04	76.9	0.519	0.680	0.63	0.02	23.3
SpSL(MM1)	0.328	0.573	0.49	1.23		0.464	0.711	0.61	2.66	
SpSL(MM2)	0.579	0.600	0.23	21.61		0.638	0.726	0.25	46.12	
N-SpSL(Exact)	0.332	0.598	0.52	0.03	5412.8	0.524	0.665	0.60	0.02	1109.0
N-SpSL(RW)	0.332	0.597	0.52	0.03	1467.1	0.524	0.665	0.60	0.02	343.3
N-SpSL(MAP)	0.282	0.650	0.61	0.75		0.291	0.829	0.81	0.86	
EMVS	0.390	0.642	0.50	3.19		0.487	0.721	0.50	2.80	
SSLasso	0.400	0.531	0.51	1.52		0.657	0.588	0.56	3.99	
HS	0.257	0.687	0.63	0.18	150.6	0.373	0.775	0.74	0.08	44.7
N-HS(RW)	0.258	0.686	0.62	0.19	646.3	0.374	0.774	0.74	0.08	156.5
BL	0.268	0.693	0.60	3.10	1180.1	0.327	0.807	0.80	2.69	330.5
N-BL(RW)	0.234	0.712	0.67	1.16	743.1	0.301	0.821	0.83	0.65	223.8
N-BL(MAP)	0.247	0.694	0.59	2.19		0.280	0.835	0.80	2.53	
Lasso(CV)	0.244	0.686	0.46	6.96		0.316	0.815	0.47	20.19	
SCAD(CV)	0.357	0.614	0.41	4.89		0.367	0.800	0.50	12.74	
Lasso(BIC)	0.356	0.541	0.56	0.60		0.568	0.635	0.67	1.74	
SCAD(BIC)	0.385	0.524	0.52	0.89		0.628	0.602	0.59	2.97	

Table 3: Results for the low-dimensional setting with dependent covariates.

Method	Weak Signal ($s = 1$)									
	$(n = 100, p = 300)$					$(n = 150, p = 1000)$				
	MSE	Angle	MCC	FP	ESS	MSE	Angle	MCC	FP	ESS
SpSL	0.443	0.806	0.73	0.00	11.2	0.193	0.920	0.89	0.00	3.3
SpSL(MM1)	0.728	0.670	0.58	2.50		1.298	0.397	0.28	6.74	
SpSL(MM2)	1.708	0.465	0.22	46.84		2.551	0.252	0.10	82.13	
N-SpSL(Exact)	0.435	0.815	0.73	0.00	181.9	0.190	0.923	0.89	0.00	29.6
N-SpSL(RW)	0.474	0.801	0.70	0.00	43.1	0.209	0.915	0.87	0.00	7.2
N-SpSL(MAP)	0.250	0.899	0.87	0.61		0.146	0.944	0.90	1.11	
EMVS	0.928	0.642	0.64	0.12		0.822	0.602	0.55	0.20	
SSLasso	0.857	0.629	0.64	0.32		0.407	0.819	0.85	0.28	
HS	0.309	0.878	0.86	0.33	27.8	0.127	0.951	0.95	0.23	4.4
N-HS(RW)	0.308	0.879	0.86	0.32	20.6	0.127	0.951	0.95	0.21	2.9
BL	0.790	0.617	0.50	14.02	67.6	0.875	0.562	0.79	1.74	5.7
N-BL(RW)	0.650	0.706	0.72	3.06	29.7	0.690	0.704	0.85	0.37	3.4
N-BL(MAP)	0.430	0.821	0.35	30.36		0.334	0.870	0.29	50.13	
Lasso(CV)	0.447	0.830	0.42	23.46		0.330	0.899	0.41	29.44	
SCAD(CV)	0.329	0.875	0.45	18.91		0.203	0.924	0.38	32.69	
Lasso(BIC)	1.138	0.576	0.63	0.01		0.947	0.718	0.83	0.01	
SCAD(BIC)	1.138	0.581	0.64	0.00		0.947	0.718	0.83	0.01	
Method	Strong Signal ($s = 1.5$)									
	$(n = 100, p = 300)$					$(n = 150, p = 1000)$				
	MSE	Angle	MCC	FP	ESS	MSE	Angle	MCC	FP	ESS
SpSL	0.089	0.986	0.99	0.02	12.6	0.037	0.995	1.00	0.02	3.4
SpSL(MM1)	0.489	0.909	0.82	1.58		1.932	0.613	0.43	8.35	
SpSL(MM2)	2.122	0.644	0.26	45.60		4.150	0.317	0.11	87.16	
N-SpSL(Exact)	0.096	0.985	0.98	0.03	314.9	0.040	0.994	1.00	0.02	40.3
N-SpSL(RW)	0.109	0.983	0.98	0.02	69.1	0.042	0.994	1.00	0.01	9.9
N-SpSL(MAP)	0.104	0.984	0.97	0.37		0.083	0.987	0.95	0.58	
EMVS	0.560	0.908	0.98	0.04		0.373	0.936	0.96	0.12	
SSLasso	0.219	0.962	0.95	0.40		0.048	0.993	0.94	0.68	
HS	0.103	0.984	0.97	0.33	29.5	0.053	0.992	0.98	0.25	5.0
N-HS(RW)	0.103	0.984	0.97	0.33	27.7	0.053	0.992	0.98	0.25	3.4
BL	1.041	0.815	0.62	9.66	54.7	1.452	0.751	0.92	0.98	4.7
N-BL(RW)	0.731	0.894	0.88	1.74	25.3	0.937	0.881	0.98	0.12	3.0
N-BL(MAP)	0.394	0.941	0.36	30.40		0.332	0.955	0.30	48.70	
Lasso(CV)	0.412	0.947	0.44	24.25		0.332	0.965	0.40	33.72	
SCAD(CV)	0.153	0.975	0.53	13.72		0.095	0.985	0.50	18.09	
Lasso(BIC)	1.740	0.821	0.96	0.08		1.577	0.861	0.99	0.05	
SCAD(BIC)	1.690	0.825	0.96	0.08		1.568	0.859	0.99	0.05	

Table 4: Results for the high-dimensional setting with independent covariates.

Method	Weak Signal ($s = 1$)									
	$(n = 100, p = 300)$					$(n = 150, p = 1000)$				
	MSE	Angle	MCC	FP	ESS	MSE	Angle	MCC	FP	ESS
SpSL	0.962	0.603	0.54	0.04	9.6	0.908	0.620	0.57	0.02	2.0
SpSL(MM1)	1.022	0.519	0.45	1.05		1.282	0.380	0.32	2.77	
SpSL(MM2)	2.026	0.378	0.17	39.57		2.423	0.277	0.10	70.98	
N-SpSL(Exact)	0.918	0.606	0.53	0.03	284.0	0.873	0.633	0.57	0.01	35.8
N-SpSL(RW)	0.911	0.604	0.53	0.03	69.3	0.878	0.626	0.57	0.01	9.1
N-SpSL(MAP)	0.891	0.610	0.56	0.61		0.807	0.641	0.58	1.22	
EMVS	1.563	0.479	0.52	0.27		0.961	0.523	0.56	0.27	
SSLasso	1.188	0.496	0.50	0.25		1.100	0.534	0.53	0.48	
HS	0.816	0.647	0.61	0.29	29.7	0.777	0.663	0.65	0.22	4.8
N-HS(RW)	0.818	0.646	0.61	0.30	26.8	0.773	0.664	0.64	0.21	3.4
BL	0.900	0.537	0.53	6.93	73.9	0.895	0.517	0.70	1.02	6.1
N-BL(RW)	0.814	0.595	0.64	1.74	33.7	0.823	0.573	0.70	0.25	3.9
N-BL(MAP)	0.786	0.619	0.29	19.63		0.727	0.636	0.25	35.48	
Lasso(CV)	0.782	0.636	0.43	10.81		0.717	0.664	0.39	16.52	
SCAD(CV)	1.027	0.575	0.34	9.80		1.000	0.587	0.34	13.69	
Lasso(BIC)	1.186	0.476	0.50	0.04		1.165	0.497	0.55	0.04	
SCAD(BIC)	1.183	0.476	0.49	0.06		1.178	0.493	0.54	0.05	
Method	Strong Signal ($s = 1.5$)									
	$(n = 100, p = 300)$					$(n = 150, p = 1000)$				
	MSE	Angle	MCC	FP	ESS	MSE	Angle	MCC	FP	ESS
SpSL	1.401	0.743	0.69	0.03	10.9	1.007	0.810	0.78	0.01	2.6
SpSL(MM1)	2.106	0.577	0.50	1.36		2.143	0.544	0.44	2.24	
SpSL(MM2)	2.731	0.529	0.22	36.81		3.597	0.372	0.12	66.82	
N-SpSL(Exact)	1.353	0.746	0.68	0.02	197.1	1.004	0.816	0.76	0.01	25.9
N-SpSL(RW)	1.426	0.726	0.66	0.01	53.1	1.130	0.785	0.74	0.01	7.4
N-SpSL(MAP)	1.038	0.795	0.76	0.35		0.740	0.861	0.83	0.54	
EMVS	1.885	0.664	0.71	0.28		1.473	0.679	0.69	0.23	
SSLasso	2.172	0.591	0.60	0.19		1.636	0.678	0.66	0.45	
HS	1.109	0.793	0.79	0.27	29.4	0.785	0.856	0.85	0.27	4.1
N-HS(RW)	1.109	0.794	0.78	0.26	21.3	0.794	0.854	0.85	0.28	2.6
BL	1.555	0.667	0.59	8.56	68.2	1.744	0.612	0.71	1.76	5.5
N-BL(RW)	1.402	0.718	0.73	1.75	31.3	1.606	0.662	0.75	0.42	3.7
N-BL(MAP)	1.204	0.758	0.35	21.03		1.223	0.760	0.28	37.99	
Lasso(CV)	1.240	0.759	0.46	14.56		1.258	0.762	0.38	26.23	
SCAD(CV)	1.484	0.731	0.39	12.40		1.338	0.752	0.36	21.14	
Lasso(BIC)	2.422	0.544	0.62	0.00		2.311	0.562	0.65	0.08	
SCAD(BIC)	2.467	0.537	0.60	0.07		2.383	0.547	0.61	0.14	

Table 5: Results for the high-dimensional setting with dependent covariates.

5.3 Results discussion

Table 2 and Table 3 summarize the results of the low-dimensional simulation studies with both independent and AR(1) covariance structures for the predictors. We first note that no procedure clearly dominated others in all situations for all criteria. Neuronized priors performed quite well and robustly throughout all situations in comparison with their counterparts, with much improved computational efficiency, except for the neuronoized Bayesian Lasso. Overall, the MAP estimator based on the neuronized SpSL prior performed comparably or best in the settings with independent covariates, and the horseshoe prior and its neuronized version also showed comparable performance in estimation and model selection, to the neuronized SpSL prior. Under the dependent structure on covariates, the neuronized Bayesian Lasso performed better than others, while the Lasso-like procedures showed similar performances.

The results also show that the results of Lasso and SCAD are sensitive to the choice of the tuning parameters. While Lasso and SCAD with the tuning parameter chosen by a 10-folded cross-validation attained comparable estimation performance (small MSE and large angle value), the procedures based on BIC showed the largest MSE and the lowest angle value. On the other hand, in terms of variable selection performance, the results are the opposite. The BIC-based Lasso and SCAD performed much better than their CV-based counterparts, i.e., the MCC was higher and the number of false positives was smaller. These results are related to the bias of the Lasso and the SCAD penalty as discussed in Rockova & George (2018). The tuning parameter chosen by BIC is highly likely to be larger than the value chosen by the CV procedure. Consequently, the strength of shrinkage is likely so strong that even significant signals are over-regularized. This bias of the penalty results in worse estimation performances. On the other hand, a strong regularization by a large tuning parameter reduces the number of false positives so that the model selection performance is improved in light of the loss of estimation accuracy.

Table 4 and Table 5 show the simulation results for high-dimensional settings with independent and dependent covariates, respectively. Overall, when the predictors are independently generated, the procedures based on the discrete SpSL prior and the horseshoe prior performed better than other procedures in terms of MSE and MCC. Their neuronized versions also showed similar performances. When the predictors are generated from the AR(1) dependence structure with the weak signal, the Lasso-like procedures show the best estimation performance. However, when the signal is strong, the procedure based on the discrete SpSL prior and the horseshoe prior, including their neuronized versions, achieved smaller MSEs and larger MCCs compared to Lasso-like procedures.

We also make a comparison among the optimization-based SpSL procedures including the MAP estimator of the neuronized SpSL prior, the MM algorithm, EMVS, and SSLasso. The results show that in overall, the neuronized MAP estimator outperforms the other SpSL procedures. The MAP estimator approximated by the MM algorithm with $\tau_3 = 10^{-2}$ performed comparably to the neuronized MAP estimator under the low-dimensional scenarios. For the high-dimensional settings, however, its performance was significantly worse than the neuronized MAP estimator. When $n = 150$ and $p = 1000$ with independent covariates, the MM algorithm resulted in 23 times larger MSE, and its MCC was less than half of that of the neuronized procedure. SSLasso also showed a comparable performance, but slightly worse, to the neuronized MAP estimator in some scenarios. However, in the low-dimensional scenarios with $n = 400$ and $p = 100$, the MSE of SSLasso was two times larger for the weak signal case and about four times larger for the strong signal case than that of the neuronized estimator.

In terms of ESS per unit time (second), the procedures based on the neuronized priors showed an advantage over their standard counterparts. In particular for the discrete SpSL priors, compared to the standard MCMC procedure previously described, Algorithm 1 for the neuronized prior achieved at least 14.1 times and 2.2 times larger ESS in the low-dimensional scenarios and high-dimensional scenarios, respectively. The MCMC algorithm using the exact conditional sampling for α_j described in Proposition 4.1 collected at least 3.5 times more ESS than Algorithm 1 in the considered simulation examples. Compared to the standard procedure, the MCMC algorithm based on Proposition 4.1 is at least 9.0 times more efficient in terms of ESS in high-dimensional scenarios. The neuronized version of the horseshoe prior produced at least 3.5 times more ESS in low-dimensional scenarios than the standard horseshoe procedure, but produced less ESS than or comparable ESS to that of the standard one in high-dimensional scenarios. For the Bayesian Lasso procedures, the ESS of the neuronized version was significantly smaller than that of the standard Bayesian Lasso in both low and high-dimensional scenarios.

6 Real Data Examples

In this section, we consider the Boston housing data set and the Bardet-Biedl data set. The Boston housing data set was introduced in Section 2. The Bardet-Biedl data set contains the microarrays from eye tissue of 120 twelve-week old male rats. A total of 31,042 different probe sets were used to analyze the RNA from the tissue. The intensity values were normalized using the robust multi-chip averaging method (Irizarry et al. 2003).

This microarray data set has been considered in multiple articles including Huang et al. (2008), Kim et al. (2008) and Fan et al. (2011). As in those papers we are interested in finding a subset of the probe sets that are associated with the probe set *1389163_at* corresponding to the expression of gene *TRIM32*. This gene is identified to be related to Bardet-Biedl syndrome, which is a hereditary disease of retina. All other probe sets are ranked according to the absolute value of the marginal correlation to *1389163_at*, and then the top 200 probe sets are used in the analysis ($n = 120$ and $p = 200$). This data set is available in R package **flare**.

Figure 7 displays comparisons between the computational performances of the Bayesian regression using the standard priors (the discrete SpSL prior and the horseshoe prior) and their neuronized versions. These boxplots of ESS are evaluated from 50 independent MCMC chains at the actual computation time of 5, 10, and 20 seconds, respectively. The first row of figures shows the results for using the discrete SpSL and its neuronized version, while the second row shows the results for using the horseshoe prior and its neuronized version. The left panels are for the Boston hoursing data set and the right panels are for the Bardet-Biedl data set. While the procedures based on the neuronized priors have relatively larger variations on ESS in the Bardet-Biedl example, Figure 7 shows that the MCMC algorithm for the neuronized version is clearly more efficient than the standard procedure in terms of ESS in both the Boston housing data set (Figure 7 (a) and (c)) and the Bardet-Biedl data set (Figure 7 (c) and (d)). They show that in both datasets using neuronized priors helped in improving computational efficiencies. In particular, Figure 7 (b) shows that the median of ESS for the “Exact” sampling procedure using neoronized prior is about 25.9 times that of the MCMC procedure using the standard SpSL prior (5629.5 versus 217.2) at 20 second. One remark is that Figure 7(a) shows that the ESS collected from the RWMH-based algorithm for the Boston housing data example is larger than that using exact conditional sampling of α_j . We think that this result stems from the fact that the naive random walk samples of α_j come from the marginal posterior density that is free of w_j , whereas the exact sampling scheme takes advantage of the explicit form as in Proposition 4.1 given w_j . In low-dimensional cases, the advantage of this exact conditional sampling might be insufficient to offset damages due to the high correlation between α_j and w_j .

Figure 7 (c) and (d) show the boxplots of ESS collected by the MCMC algorithms based on the standard horseshoe prior and its neuronized version (Section 2), respectively. For the Boston housing data set, the ESS of the neuronized version is 50% larger than that of the standard horseshoe prior. For the Bardet-Biedl data set, the neuronized version collects about 10% more effective samples compared to the horseshoe prior.

For the Bardet-Biedl data set, Figure 8 shows the trace plots of the logarithm of the

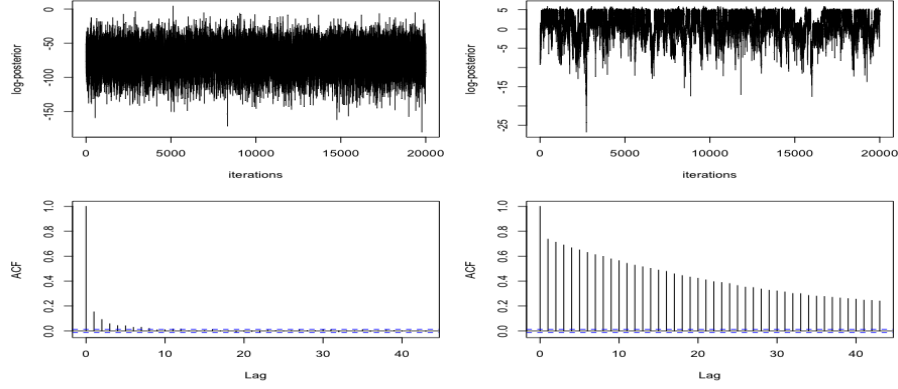


Figure 8: Trace plots and autocorrelation plots of the logarithm of the posterior density evaluated at the MCMC samples for the neuronized SpSL(first column) and the standard SpSL(second column) for the Bardet-Biedl data set.

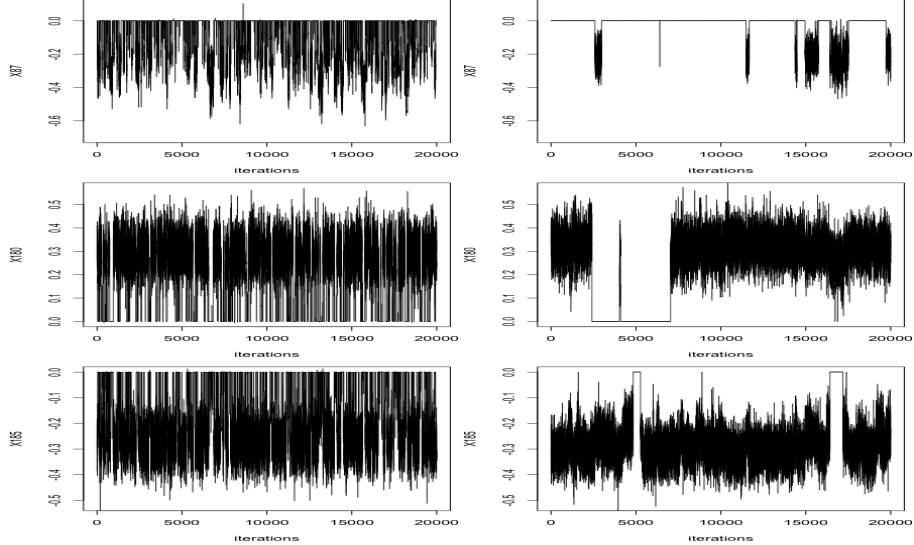


Figure 9: For the Bardet-Biedl data set, trace plots of some significant coefficients for X_{87} (top), X_{180} (middle), and X_{185} (bottom). The left column contains MCMC chains based on the neuronized discrete SpSL prior, and the right column includes MCMC chains based on the standard discrete SpSL prior.

posterior density evaluated at posterior samples based on the standard SpSL prior and its neuronized version (thinning size is 10). The mixing results are consistent with the results shown in Figure 7. The MCMC chain for the neuronized version achieves much better mixing performance compared to the procedure using the standard SpSL prior. This computational superiority is confirmed again in the trace plots of individual coefficients in Figure 9. In the trace plot of the regression coefficient corresponding to X_{87} , the MCMC chain based on the discrete SpSL prior does not mix well, getting stuck at zero more than its fair share. For the coefficients of X_{180} and X_{185} , the procedure for using the standard SpSL are also shown to be quite sticky. In contrast, the MCMC chain of the neuronized version efficiently switches between zero and non-zero values.

Method	Boston housing			Bardet-Biedl		
	MSPE	Angle	MS	MSPE	Angle	MS
SpSL	25.299	0.840	5.29	0.508	0.699	2.44
SpSL(MM1)	27.341	0.826	4.81	0.502	0.669	5.63
SpSL(MM2)	25.538	0.839	7.00	0.497	0.614	46.41
N-SpSL(Exact)	25.098	0.842	5.88	0.501	0.704	1.84
N-SpSL(RW)	25.097	0.842	5.88	0.501	0.704	1.82
N-SpSL(MAP)	25.045	0.843	6.40	0.479	0.696	4.20
EMVS	43.824	0.739	4.37	0.477	0.676	11.79
SSLasso	87.125	0.601	6.88	0.473	0.685	17.73
HS	25.122	0.842	6.03	0.447	0.711	3.76
N-HS(RW)	25.137	0.842	6.04	0.448	0.710	3.73
BL	25.185	0.842	6.65	0.369	0.698	20.77
N-BL(RW)	25.167	0.842	6.19	0.387	0.716	15.47
N-BL(MAP)	25.192	0.842	6.59	0.432	0.705	12.00
Lasso(CV)	25.196	0.842	8.60	0.424	0.707	22.59
SCAD(CV)	25.111	0.842	7.31	0.491	0.694	9.77
Lasso(BIC)	26.833	0.833	7.09	1.176	0.665	2.07
SCAD(BIC)	25.515	0.839	6.34	1.157	0.655	2.25

Table 6: Results for the synthesized real datasets. “MSPE” and “MS” indicate the out-of-sample prediction error and the average number of selected variables, respectively.

We consider the out-of-sample mean squared prediction error (MSPE) to measure the prediction performance of each procedure. To evaluate this quantity, we randomly split 10% of the samples as test samples, and estimate the regression coefficients by using the other 90% samples, then we evaluate the MSPE and the angle by comparing the test samples and the predicted values over 100 replicates. The same settings of hyperparameter and computational strategies used in the simulation studies are applied for this comparison.

In Table 6, the results show that the neuronized versions performed comparably with their standard counterparts for the real data sets. For the Boston housing data set, the MAP estimator with the neuronized SpSL prior had the smallest prediction error and angle. We note that the MSPE of SSLasso is more than three times larger than that of other procedures. For the Bardet-Biedl data set, the Bayesian Lasso and neuronized Bayesian Lasso performed better in prediction than others.

7 Conclusion

Inspired by the idea of neuron activation, which is central to all neural network (aka deep learning) methods, we propose to use an activation function and a product representation to unify and extend shrinkage priors employed in high-dimensional Bayesian regression analyses. By simply changing the activation function, our unified framework (and its companion software package) enables practitioners to easily test out the effects of imposing different classes of priors for their regression models. Furthermore, our “neronization” formulation of the prior distribution enables us to develop more efficient MCMC sampling algorithms for the full Bayesian inference. For example, we show empirically that the MCMC algorithm based on the neuronized version of the discrete SpSL prior is about 5-10 times more efficient than the standard procedure in terms of ESS.

We note that the currently available strategy for Bayesian inference with the discrete SpSL prior is quite sophisticated and nontrivial, as it requires one to integrate out all continuous coefficients conditioning on the variable inclusion indicator vector. This integration strategy, however, is no longer available if a non-conjugate prior is used, or the linear regression is changed to, say, the logistic regression or other generalized linear models. In contrast, the adoption of the neuronized prior formulation renders the integration strategy unnecessary and makes it much more practical to use the discrete SpSL prior (neuronized version) for the full Bayesian analysis of a broad class of statistical models (e.g., logistic regression models).

Since the neuronized prior contains only continuous parameters, not discrete ones, an efficient optimization algorithm can be developed to find the posterior mode (the MAP estimator) of a regression model without considering additional computational strategies such as the EM algorithm. For example, instead of using a Monte Carlo annealing type algorithm to solve a combinatorial optimization problem so as to find the best model under a discrete SpSL prior (or according to the BIC criterion), we illustrate how a coordinate-ascent algorithm can be used to find the MAP estimator efficiently.

Acknowledgment

This research is supported in part by the NSF grant DMS-1613035 and the NIH grant R01 HG008927-01A1.

References

Armagan, A., Dunson, D. & Lee, J. (2013), ‘Generalized double Pareto shrinkage’, *Statistica Sinica* **23**(1), 119–143.

Berger, J. O. & Molina, G. (2005), ‘Posterior model probabilities via path-based pairwise priors’, *Statistica Neerlandica* **59**(1), 3–15.

Bhattacharya, A., Chakraborty, A. & Mallick, B. K. (2016), ‘Fast sampling with gaussian scale-mixture priors in high-dimensional regression’, *Biometrika* **103**(4), 985.

Bhattacharya, A., Pati, D., Pillai, N. S. & Dunson, D. B. (2015), ‘Dirichlet-Laplace priors for optimal shrinkage’, *J. Am. Statist. Ass.* **110**(512), 1479–1490.

Brent, R. P. (1973), *Algorithms for minimization without derivatives*, Prentice-Hall.

Brown, P. J., Vannucci, M. & Fearn, T. (1998), ‘Bayesian wavelength selection in multi-component analysis’, *Journal of Chemometrics* **12**(3), 173–182.

Carvalho, C., Polson, N. & Scott, J. (2010), ‘The horseshoe estimator for sparse signals’, *Biometrika* **97**(2), 465–480.

Castillo, I., Schmidt-Hieber, J., Van der Vaart, A. et al. (2015), ‘Bayesian linear regression with sparse priors’, *Ann. Statist.* **43**(5), 1986–2018.

Castillo, I., van der Vaart, A. et al. (2012), ‘Needles and straw in a haystack: Posterior concentration for possibly sparse sequences’, *Ann. Statist.* **40**(4), 2069–2101.

Chen, J. & Chen, Z. (2008), ‘Extended Bayesian information criteria for model selection with large model spaces’, *Biometrika* **95**(3), 759–771.

URL: <http://biomet.oxfordjournals.org/cgi/doi/10.1093/biomet/asn034>

Dekker, T. (1969), ‘Finding a zero by means of successive linear interpolation’, *Constructive aspects of the fundamental theorem of algebra* pp. 37–51.

Dellaportas, P., Forster, J. J. & Ntzoufras, I. (2002), ‘On Bayesian model and variable selection using mcmc’, *Statistics and Computing* **12**(1), 27–36.

Fan, J., Feng, Y. & Song, R. (2011), ‘Nonparametric independence screening in sparse ultra-high-dimensional additive models’, *J. Am. Statist. Ass.* **106**(494), 544–557.

Fan, J. & Li, R. (2001), ‘Variable selection via nonconcave penalized likelihood and its oracle properties’, *J. Am. Statist. Ass.* **96**(456), 1348–1360.

Fischer, A. (1992), ‘A special newton-type optimization method’, *Optimization* **24**(3–4), 269–284.

Gelman, A. (2006), ‘Prior distributions for variance parameters in hierarchical models’, *Bayesian Analysis* **1**(3), 515–533.

George, E. I. & McCulloch, R. E. (1997), ‘Approaches for Bayesian variable selection’, *Statistica Sinica* **7**(2), 339–373.

George, E. & McCulloch, R. (1993), ‘Variable selection via Gibbs sampling’, *J. Am. Statist. Ass.* **88**(423), 881–889.

Ghosh, P., Chakrabarti, A. et al. (2017), ‘Asymptotic optimality of one-group shrinkage priors in sparse high-dimensional problems’, *Bayesian Analysis* **12**(4), 1133–1161.

Glorot, X., Bordes, A. & Bengio, Y. (2011), Deep sparse rectifier neural networks, in ‘Proceedings of the Fourteenth International Conference on Artificial Intelligence and Statistics’, pp. 315–323.

Green, P. J. (1995), ‘Reversible jump markov chain monte carlo computation and bayesian model determination’, *Biometrika* pp. 711–732.

Guan, Y. & Stephens, M. (2011), ‘Bayesian variable selection regression for genome-wide association studies and other large-scale problems’, *Ann. Appl. Statist.* pp. 1780–1815.

Hahn, P. R. & Carvalho, C. M. (2015), ‘Decoupling shrinkage and selection in Bayesian linear models: a posterior summary perspective’, *J. Am. Statist. Ass.* **110**(509), 435–448.

Hans, C., Dobra, A. & West, M. (2007), ‘Shotgun stochastic search for large p regression’, *J. Am. Statist. Ass.* **102**(478), 507–516.

Hoff, P. D. (2017), ‘Lasso, fractional norm and structured sparse estimation using a hadamard product parametrization’, *Computational Statistics & Data Analysis* **115**, 186–198.

Huang, J., Ma, S. & Zhang, C.-H. (2008), ‘Adaptive lasso for sparse high-dimensional regression models’, *Statistica Sinica* pp. 1603–1618.

Irizarry, R. A., Hobbs, B., Collin, F., Beazer-Barclay, Y. D., Antonellis, K. J., Scherf, U. & Speed, T. P. (2003), ‘Exploration, normalization, and summaries of high density oligonucleotide array probe level data’, *Biostatistics* **4**(2), 249–264.

Johnson, V. E. & Rossell, D. (2010), ‘On the use of non-local prior densities in Bayesian hypothesis tests’, *J. R. Statist. Soc. B* **72**(2), 143–170.

Johnson, V. E. & Rossell, D. (2012), ‘Bayesian model selection in high-dimensional settings’, *J. Am. Statist. Ass.* **107**(498), 649–660.

Kim, Y., Choi, H. & Oh, H.-S. (2008), ‘Smoothly clipped absolute deviation on high dimensions’, *J. Am. Statist. Ass.* **103**(484), 1665–1673.

Kirkpatrick, S. & Vecchi, M. (1983), ‘Optimization by simulated annealing’, *Science* **220**(4598), 671–680.

Madigan, D., York, J. & Allard, D. (1995), ‘Bayesian graphical models for discrete data’, *International Statistical Review/Revue Internationale de Statistique* pp. 215–232.

Matthews, B. W. (1975), ‘Comparison of the predicted and observed secondary structure of t4 phage lysozyme’, *Biochimica et Biophysica Acta (BBA)-Protein Structure* **405**(2), 442–451.

Mitchell, T. J. & Beauchamp, J. J. (1988), ‘Bayesian variable selection in linear regression’, *J. Am. Statist. Ass.* **83**(404), 1023–1032.

Narisetty, N. N. & He, X. (2014), ‘Bayesian variable selection with shrinking and diffusing priors’, *Ann. Statist.* **42**(2), 789–817.

URL: <http://projecteuclid.org/euclid-aos/1400592178>

Park, T. & Casella, G. (2008), ‘The Bayesian lasso’, *J. Am. Statist. Ass.* **103**(482), 681–686.

Piironen, J. & Vehtari, A. (2017), On the hyperprior choice for the global shrinkage parameter in the horseshoe prior, in ‘Artificial Intelligence and Statistics’, pp. 905–913.

Polson, N. & Scott, J. (2010), Shrink globally, act locally: sparse Bayesian regularization and prediction, in 'Proceedings of the 9th Valencia World Meeting on Bayesian Statistics', Vol. 9, Oxford University Press, pp. 501–538.

Polson, N., Scott, J. & Windle, J. (2013), 'Bayesian inference for logistic models using polya–gamma latent variables', *J. Am. Statist. Ass.* **108**(504), 1339–1349.

Raftery, A. E., Madigan, D. & Hoeting, J. A. (1997), 'Bayesian model averaging for linear regression models', *J. Am. Statist. Ass.* **92**(437), 179–191.

Rockova, V. & George, E. I. (2014), 'EMVS: The EM approach to Bayesian variable selection', *J. Am. Statist. Ass.* **109**(506), 828–846.

Rockova, V. & George, E. I. (2018), 'The spike-and-slab lasso', *J. Am. Statist. Ass.* **113**(521), 431–444.

Rosenblatt, F. (1958), 'The perceptron: a probabilistic model for information storage and organization in the brain.', *Psychological review* **65**(6), 386.

Rossell, D. & Telesca, D. (2017), 'Non-local priors for high-dimensional estimation', *J. Am. Statist. Ass.* (just-accepted).

Rumelhart, D. E., Hinton, G. E. & Williams, R. J. (1986), 'Learning representations by back-propagating errors', *Nature* **323**(6088), 533.

Scott, J. & Berger, J. (2010), 'Bayes and empirical-Bayes multiplicity adjustment in the variable-selection problem', *Ann. Statist.* **38**(5), 2587–2619.

Tibshirani, R. (1996), 'Regression shrinkage and selection via the lasso', *J. R. Statist. Soc. B* pp. 267–288.

Tseng, P. & Yun, S. (2009), 'A coordinate gradient descent method for nonsmooth separable minimization', *Mathematical Programming* **117**(1-2), 387–423.

van der Pas, S., Kleijn, B., van der Vaart, A. et al. (2014), 'The horseshoe estimator: Posterior concentration around nearly black vectors', *Electronic Journal of Statistics* **8**(2), 2585–2618.

van der Pas, S., Salomond, J.-B., Schmidt-Hieber, J. et al. (2016), 'Conditions for posterior contraction in the sparse normal means problem', *Electronic Journal of Statistics* **10**(1), 976–1000.

Yang, Y., Wainwright, M. J. & Jordan, M. I. (2016), ‘On the computational complexity of high-dimensional bayesian variable selection’, *Ann. Statist.* **44**(6), 2497–2532.

Yen, T.-J. et al. (2011), ‘A majorization–minimization approach to variable selection using spike and slab priors’, *Ann. Statist.* **39**(3), 1748–1775.

Zellner, A. (1986), On assessing prior distributions and Bayesian regression analysis with g-prior distributions, in ‘Bayesian inference and decision techniques: Essays in Honor of Bruno de Finetti’, North Holland, Amsterdam, pp. 233–243.

Zhang, J. L., Lin, M. T., Liu, J. S. & Chen, R. (2007), ‘Lookahead and piloting strategies for variable selection’, *Statistica Sinica* **17**(3), 985–1003.

URL: <http://www.jstor.org/stable/24307709>

Appendix: Proofs of Main Results

Proof of Lemma 2.1. Let $\theta = \alpha w$ and $z = w$. By a change of variable, the Jacobian term is z^{-1} , and a simple plug-in of $\alpha = \theta/z$ and $w = z$ completes the proof. \square

Proof of Proposition 2.2. We first show that the lower bound holds. By a change of variable $u = z^2$, for any $0 < \epsilon < 1$,

$$\begin{aligned}\pi_L(\theta) &= \int_0^\infty z^{-1} \exp\{-\theta^2/(2\tau_w^2 z^2) - z^2/2\} dz \\ &= (2\tau_w^2)^{-1} \int_0^\infty u^{-1} \exp\{-\theta^2/(2\tau_w^2 u) - u/2\} du \\ &= (2\tau_w^2)^{-1} \int_0^\infty u^{-1/2} \exp\{\epsilon u/2\} u^{-1/2} \exp\{-\theta^2/(2\tau_w^2 u) - (1/2 + \epsilon/2)u\} du \\ &\geq (2\tau_w^2)^{-1} \epsilon^{1/2} \exp\{1\} \int_0^\infty u^{-1/2} \exp\{-\theta^2/(2\tau_w^2 u) - (1/2 + \epsilon/2)u\} du \\ &= (2\tau_w^2)^{-1} \epsilon^{1/2} \exp\{1\} (\pi/(1/2 + \epsilon/2))^{1/2} \exp\{-(1 + \epsilon)^{1/2}|\theta|/\tau_w\}.\end{aligned}$$

Second, we show that the upper bound holds.

$$\begin{aligned}\pi_L(\theta) &= \int_0^\infty z^{-1} \exp\{-\theta^2/(2\tau_w^2 z^2) - z^2/2\} dz \\ &\geq \int_0^\infty \exp\{-(1 - \epsilon)\theta^2/(2\tau_w^2 z^2) - z^2/2\} dz \\ &\propto \exp\{-(1 - \epsilon)^{1/2}|\theta|/\tau_w\}.\end{aligned}$$

\square

Proof of Proposition 2.3. Let $z = w$ and without loss of generality, assume that $\theta > 0$. Because the tail behavior of θ is governed by the positive region of α , we assume that $\alpha > 0$. Then, the marginal density can be expressed by a change of variable as

$$\int_{-\infty}^\infty \frac{z}{\lambda_1 \theta} \left\{ \frac{\lambda_2^2}{\lambda_1^2} + \frac{\log(\theta/z)}{\lambda_1} \right\}^{-1/2} \exp \left\{ -\frac{1}{2} \left[\frac{\lambda_2}{\lambda_1} + \left\{ \frac{\lambda_2^2}{\lambda_1^2} + \frac{\log(\theta/z)}{\lambda_1} \right\}^{1/2} \right]^2 - \frac{z^2}{2} \right\} dz.$$

By the *dominated convergence theorem*, for a large $\theta > 0$, it follows that

$$\pi_E(\theta) \approx c \int_{-\infty}^\infty \log(\theta/z)^{-1/2} \theta^{-1/(2\lambda_1)-1} \exp \left\{ \frac{z^2}{2\tau_w^2} \right\} dz,$$

for some positive constant c . This result completes the proof. \square

Proof of Proposition 4.1. We note that the conditional posterior density of α_j given the others is

$$\pi(\alpha_j | \alpha_{(-j)}, w, \sigma^2, \mathbf{y}) \propto (2\pi)^{-1/2} \exp \left\{ -\frac{\|r_j - X_j T(\alpha_j - \alpha_0)w_j\|_2^2}{2\sigma^2} - \frac{\alpha_j^2}{2} \right\}.$$

Since the activation function is the ReLU function, it follows that

$$\pi(\alpha_j | \alpha_{(-j)}, w, \sigma^2, \mathbf{y}) \propto \begin{cases} (2\pi)^{-1/2} \exp \left\{ -\|r_j\|_2^2/(2\sigma^2) - \alpha_j^2/2 \right\}, & \text{if } \alpha_j < \alpha_0 \\ (2\pi)^{-1/2} \exp \left\{ -\|\tilde{r}_j - X_j \alpha_j w_j\|_2^2/(2\sigma^2) - \alpha_j^2/2 \right\}, & \text{if } \alpha_j \geq \alpha_0, \end{cases}$$

where $\tilde{r}_j = r_j + X_j \alpha_0 w_j$. By doing a simple calculation, it follows that

$$\begin{aligned} & (2\pi)^{-1/2} \exp \left\{ -\|\tilde{r}_j - X_j \alpha_j w_j\|_2^2/(2\sigma^2) - \alpha_j^2/2 \right\} \\ &= \tilde{\sigma}_j \exp \left\{ -\|\tilde{r}_j\|_2^2/(2\sigma^2) + \tilde{\alpha}_j^2/(2\tilde{\sigma}_j^2) \right\} \phi(\alpha_j; \tilde{\alpha}_j, \tilde{\sigma}_j^2), \end{aligned}$$

where $\phi(\cdot; u, z)$ is the Gaussian density function with mean u and variance z , and $\tilde{\alpha}_j$ and $\tilde{\sigma}_j^2$ are defined in the statement of the proposition. This completes the proof. \square